PROTECTIVE AND FUNCTIONAL POWDER COATINGS

THERMAL BARRIER COATINGS: CURRENT STATUS, SEARCH, AND ANALYSIS

**S. M. Lakiza,[1,4] M. I. Grechanyuk,[1] O. K. Ruban,[1]
V. P. Redko,[1] M. S. Glabay,[1] O. B. Myloserdov,[2]
O. V. Dudnik,[1] and S. V. Prokhorenko[3]**

UDC 62-761

The principles for selecting materials to be used as thermal barrier coatings (TBCs) are presented. The advantages and disadvantages of new methods for TBC deposition are briefly described. After measurement of the thermal conductivity and thermal expansion coefficient, it is required to ascertain that such materials do not interact with the thermally grown aluminum oxide and then to determine their strength, fracture toughness, hardness, and Young's modulus. The thermal conductivity of TBC can be reduced by increasing its porosity and suppressing its sintering. The need for and drawbacks of multilayer coatings are shown. If TBC meets all the requirements, then TBC corrosion resistance to Na_2SO_4, V_2O_5, P_2O_5, sand, and volcanic ash in operation and ways to protect TBC against damage need to be determined. The prospects and areas for development of these techniques are outlined.

Keywords: *thermal barrier coating, bond coating, thermally grown oxide, thermal conductivity, mechanical properties, corrosion, zirconia, pyrochlores.*

INTRODUCTION

The development of ceramic coatings was started in the late 1940s and continued in the 1950s. Their use in the injectors of rocket engines X-15 and the flame tubes of gas-turbine engines began in the 1960s. Since the first papers on the testing of turbine blades with thermal barrier coatings (TBCs) in 1976 [1], the development of these coatings for engine hot sections has become an advanced area of modern materials science. The modern TBC structure is shown in Fig. 1 [2]. The structure includes a blade material, bond coating, thin Al_2O_3 layer formed when the product is operated at high temperatures, and TBC itself. The bond coating evens the difference in the thermal expansion coefficients between the blade material and TBC and produces a thin Al_2O_3 layer that prevents the transport of oxygen ions into the blade and, thus, its further oxidation. The outer ceramic coating accepts the

[1]Frantsevich Institute for Problems of Materials Science, National Academy of Sciences of Ukraine, Kyiv, Ukraine. [2]Zaporizhia Machine-Building Design Bureau *Progress*, Zaporizhia, Ukraine. [3]Lviv Polytechnic National University, Lviv, Ukraine.

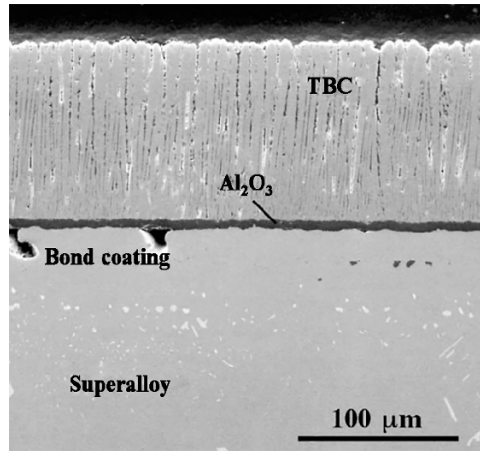[4]To whom correspondence should be addressed; e-mail: sergij_lakiza@ukr.net.

Fig. 1. Cross-section of the YSZ coating (Y_2O_3-stabilized ZrO_2) produced by electron-beam physical vapor deposition on high-temperature creep-resistant superalloys [2]

major thermal shock. Hence, the modern TBC is a complex multifunctional film from 100 μm to 2 mm in thickness to protect engine metallic parts against high-temperature gas flows.

Directionally solidified nickel superalloys (e.g., Inconel 718), which possess remarkable tension strength and high-temperature creep resistance (~1100°C) [3], are used as the gas turbine blade material. The MCrAlY alloy (M = Ni, Co, Fe), which is the first to be deposited onto the blade material, is the conventional bond coating material [3]. For the TBC itself, Y_2O_3–stabilized ZrO_2 (YSZ) as a metastable *t′* modification is used.

It is important to increase the engine operating temperature and service life. Hence, the intensive search for new materials and the improvement of deposition techniques have been on the agenda in the recent decades.

The requirements applied to new TBC materials result from many-year efforts. They are high melting point, zero phase transformations in thermal cycling at operating temperatures, low thermal conductivity, proper thermal cycling resistance, thermal expansion coefficient that corresponds to the thermal expansion of substrate materials, resistance to mechanical stresses, zero interaction of the TBC material with Al_2O_3, oxidation and corrosion resistance, and low sinterability of porous microstructures [2, 4]. The requirements are very strict. Material that would comply with all requirements and surpass conventional YSZ is still to be found. Nevertheless, the search is ongoing and a number of materials are considered to be promising [4, 5].

The development of a new TBC usually requires a number of steps:

- choose deposition materials by measuring the thermal conductivity and thermal expansion coefficient of the sinters;
- verify the chemical compatibility of the coating material with Al_2O_3, resulting from oxidation of the bond coating in the TBC performance process;
- select the coating deposition technique;
- determine the TBC mechanical properties (microhardness and fracture toughness);
- control the TBC porosity;
- determine the TBC corrosion resistance to fuel combustion products and airborne particles.

STAGES OF SEARCHING FOR AND DEVELOPING NEW TBCS

Choice of Deposition Materials by Measuring the Thermal Conductivity and Thermal Expansion Coefficient. Two groups of materials with low thermal conductivity were found and are under development [6]. These are primarily yttria-stabilized ZrO_2 (YSZ) with additions of one or several rare earth metal (REM) oxides [5, 7, 8]. The other group includes zirconates and mixed REM zirconates with pyrochlore structure [9, 10].

The literature pays significant attention to YSZ doping with a series of REM oxides [8]. Besides Y_2O_3, two other cations are added to zirconium dioxide, one with a smaller ionic radius (Yb, Sc) and the other with a larger

TABLE 1. Some Materials in the ZrO_2–Ln_2O_3 Systems Promising as TBCs for Gas Turbine Engine Blades

Material	Deposition/ production technique	Thermal conductivity, $W \cdot m^{-1} \cdot K^{-1}$	Thermal expansion coefficient α, $10^{-6} \cdot K^{-1}$	Heat resistance	Ref.
$ZrO_2 \cdot 4\%\ Gd_2O_3$	APS	2.25–2.0 (150–650°C)		The coating sinters worse, but the t' phase decomposes easier than YSZ	[14]
ZrO_2–Y_2O_3–La_2O_3	APS	1.3–1.4	9–10	50 cycles 1100–25°C	[15]
$Zr(Sm)O_2$	Chemical	1.41–1.86 (600–25°C)			[16]
$Zr(Ce,Y)$	APS		12.64–10.69 (50–900°C)	In the performance process, Ce changes its valency	[17]
$Zr(Gd)O_2$	Ceramic	2.1–1.8 (200–1000°C)			[18]
$Zr(Y,Yb)O_2$	APS	1.52–1.19			[19]
$Zr(Sc,Y)O_2$	APS			The nanostructured material has higher thermal stability than 7YSZ	[20]
$Zr(Y,Dy)O_2$	Ceramic	2.3	10.8–16 (400–900°C)		[21]

ionic radius (Sm, Nd, Gd). The so-called defect clusters emerge in such materials and are identified by scanning electron microscopy; the nanoclusters form larger and smaller REM cations, while yttrium cations are uniformly distributed [5]. These clusters effectively dissipate phonons and, hence, decrease the thermal conductivity to ~1 W/m · K. In addition, ZrO_2 doping with several cations stabilizes the coating tetragonal structure at temperatures to 1400°C and with holding for 500 h without transfer to monoclinic structure in the cooling process [11].

The replacement of some part of zirconium by hafnium, which is always present as an admixture, somewhat improves the service life of the coating and suppresses its sintering [12, 13]. Some ZrO_2–Ln_2O_3 materials for TBCs are listed in Table 1 [14–21].

Despite a number of obvious advantages, the YSZ coating has its drawbacks. The first drawback is that the upper operating temperature has its limit (1200°C) [22, 23]. The second drawback is that this type of coating is sensitive to hot corrosion [24, 25] because insufficiently pure fuel grades containing V_2O_5 and Na_2SO_4 are used. The third drawback is that the coating contains SiO_2 admixtures that diffuse along the grain boundaries in thermal cycling, concentrate at the so-called ternary points, and change the grain size and shape. Moreover, SiO_2 washes out the Y_2O_3 stabilizer from YSZ, causing its local destabilization [26]. Silicon dioxide imparts superplasticity to ZrO_2, greatly accelerating the sintering process and reducing electrical conductivity. The YSZ coating materials are characterized by highly concentrated oxygen ion vacancies, which leads to oxygen transport and oxidation of the bond coating at the bond coating/TBC interface, giving rise to thermally grown oxide. The ceramic layer delaminates as a result. This mechanism is predominant for thin gas turbine coatings. This issue was solved by developing an oxidation-resistant bond coating with use of Al_2O_3 and mullite [27].

Pyrochlore-type $A_2B_2O_7$ oxides are relatively new agents in the materials science of TBCs. The first patent was obtained in 2000 [28]. Rare earth metal zirconates with pyrochlore structure form with Ln = La–Gd. With Ln = Ho–Lu, the rhombohedral $Ln_3Zr_4O_{12}$ δ-phases form in the ZrO_2–Ln_2O_3 systems instead of pyrochlores. Both types of phases are derived from the fluorite-type structure and are superstructures relative to it [29]. The thermal barrier coatings based on some phases with pyrochlore structure are listed in Table 2 [30–56].

Besides the above materials, other oxide compounds are also promising: $Y_4Al_2O_9$ [57], $Y_3Al_5O_{12}$ [58], $HfO_2 \cdot 7.5\ Y_2O_3$ [12], $ThO_2 \cdot 8YSZ$ [60], etc. Some materials promising as TBCs and their individual properties are listed in Table 3 [57–84].

Verification of the Chemical Compatibility of the Coating Material with Thermally Grown Al_2O_3. The isothermal section of the $Al_2O_3-ZrO_2-Y_2O_3$ phase diagram at 1250°C [85, 86] (Fig. 2*a*) confirmed that YSZ can be deposited directly on the bond coating since the YSZ phase does not react with the Al_2O_3 layer formed in the performance process. This is also the case for ZrO_2 doped with several stabilizers [5].

In case of REM zirconates with pyrochlore structure, the situation is the opposite. The pyrochlores meet the main requirements for TBCs (high melting point, zero phase transformations, chemical inertness). However, the constitution of the $Al_2O_3-ZrO_2-Ln_2O_3$ phase diagrams (Ln = La, Sm, Nd, Gd) [87–93] along the isothermal sections at 1250 and 1650°C (Fig. 2*b–d*) showed that the $Ln_2Zr_2O_7$ phases reacted with Al_2O_3 to form T- or F-ZrO_2 and $LnAlO_3$. The emergence of new phases with their thermal expansion coefficients at the interface between TBC and AlO_3 leads to swelling, delamination, and destruction of the coatings in the end. The solution was proposed such as the deposition of two-layer coatings, specifically: zirconate TBC was separated from the Al_2O_3 film with a conventional YSZ layer [4]. However, this raises the question whether the phases with different thermal expansion coefficients are compatible. They cannot be ideally compatible, and even insignificant differences in the thermal expansion coefficients cause cracking with performance time and, finally, destruction of the coating. This issue can be overcome by using pyrochlore-type phases that do not interact with Al_2O_3. We associate certain hopes with lanthanum hafnates $La_2Hf_2O_7$ and REM titanates of $Ln_2Ti_2O_7$ type. The constitution of the isothermal sections of the Al_2O_3–HfO_2–La_2O_3 and Al_2O_3–TiO_2–Ln_2O_3 phase diagrams (Fig. 3) [94–96] showed that lanthanum hafnates and REM titanates did not react with Al_2O_3; hence, there is no need for two-layer TBCs that complicate the combination of thermal expansion coefficients, which would lead to coating cracking and delamination.

Thermal Barrier Coating Deposition Techniques. There are two widespread techniques for depositing the modern TBCs: electron-beam physical vapor deposition (EB-PVD) and air plasma spraying (APS). The first technique produces coatings with the longest life [97, 98] and the other technique with the lowest thermal conductivity [99, 100]. Accordingly, EB-PVD efforts were focused on reduction in the thermal conductivity to the APS values (≤ 1 W/m · K) by modifying the number and architecture of pores through variation in the process parameters. They include increase in the chamber pressure [101], increase in the distance from the vapor source in the deposition process [102], use of interrupted plasma for density modulation [103], periodic introduction of admixtures into the deposition area to terminate and renew finer columnar grow [104], and modification of substrates to acquire zigzag structure in which the gaps between the columns have oblique orientation to block heat transfer through the coating in a more effective manner [105]. The last two approaches reflect important changes in the understanding of pore architecture, where the gaps between the columns are no longer deemed to be only capable of reducing stresses [106], but also to be potential contributors to lower thermal conductivity. The minimum thermal conductivity in all these cases is, as before, ≥ 1 W/m · K.

The most radical innovation in the EB-PVD technique is probably the use of a high-speed gas flow to focus the vapor beam, known as directed vapor deposition [107]. This technique is suitable for depositing parts with complex shape.

Two aspects are noticeable in the APS technique. One of them is to produce a dense vertically cracked TBC [108]. The generation of cracks that imitate the segmentation of EB-PVD coatings increases the strain-hardening resistance [109]. The coating density can be reduced near the surface to facilitate its postcoat finishing and optimize the profile aerodynamics by varying the deposition parameters [110]. This technique is promising for large turbine components, especially combustion chambers and atomizers in the latest electric power facilities [6].

The solution precursor plasma spray is another innovation in the plasma spraying technique. This technique produces a nanostructured coating through rapid solvent evaporation, pyrolysis, and solidification, proceeding both in the air and on the substrate [111]. These data indicate that the significant improvement in the cyclic fatigue life compared to the APS and even EB-PVD techniques [112] is ensured by a dense vertically cracked microstructure. However, the thermal conductivity of these coatings is much higher than in conventional APS coatings (1.4 W/m · K) [113].

TABLE 2. Some Materials Based on Pyrochlore-Type Phases

Material	Deposition/ production technique	Thermal conductivity, $W \cdot m^{-1} \cdot K^{-1}$	Thermal expansion coefficient α, $10^{-6} \cdot K^{-1}$	Young's modulus E, GPa
$La_2Ce_2O_7$		0.32–0.5 (300–1300°C)	12.3–13	
$Ln_2Zr_2O_7 (Ln = Dy, Er, Yb)$		1.3–1.9		
$(La, Sm, Yb)_2(Zr, Ce)_2O_{7.4}$; $(Sr_{0.1}La_{0.3}Sm_{0.5}Yb_{0.1})_2$ $(Zr_{0.7}Ce_{0.4})_2O_{7.3}$	Chemical	1.32–1.3 1.17–1.16	~11	10–11
$(Nd, Yb)_2Zr_2O_7$	Chemical		10.93–10.62 (1250°C)	
$Gd_2Zr_2O_7(2.3–8.25Y_2O_3)$	Ceramic, EB-PVD	0.82–1.32	10–10.5	
$La_2Zr_2O_7 + 3$ wt.% Y_2O_3	EB-PVD		9.15–9.27	153–146
$(La_{1-x}Yb_x)_2Zr_2O_7$	Chemical	1.3		
$La_2T_2O_7$ T = Ge; Ti; Sn; Zr; Hf	First principles calculations	1.14 1.17 1.00 1.03 0.87		258 253 245 237 228
Gradient $YSZ/La_2Zr_2O_7$ six-layer coating	APS	0.65–0.74 (1200°C)	8.18–9.836	203–182
$Sm_2Zr_2O_7$	EB-PVD			
$Gd_2Ce_2O_7$ $(Gd_{0.9}Ca_{0.1})_2/Ce_2O_{6.9}$	Ceramic	3.1–2.0 2.5–1.8 (200–800 °C)		
$La_2(Zr_{0.7}Ce_{0.3})_2O_7/YSZ$	EB-PVD	Advantages: poor sinterability, close thermal expansion coefficients, and columnar structure; drawbacks: variable Ce valency		
$(Sm_{1-x}Yb_x)_2Zr_2O_7$	Chemical	~1.4 (800°C)		
$(Mg_7La_{0.5-x}Sm_{0.5})_2$ $(Zr_{0.7}Ce_{0.3})_2O_{1-x}$	Chemical	1.57 ($x = 0.2$)	11.3 (800°C)	
$La_2(Zr_xCe_{1-x})_2O_7$	Ceramic	~1.5 (1000°C)		
$La_2Zr_2O_7$ Pr Nd Sm Eu Gd	Calculations using local density approximation and Hubbard energy	1.2 1.2 1.1 1.3 1.2 1.2		208 224 213 252 243 214

Specific weight, g/cm^3	Thermal stability	K_{Ic}, MPa · m$^{0.5}$	Vickers hardness, GPa	Ref.
				[30]
Dy = 6.89 Er = 7.29 Yb = 7.54				[31]
				[32]
				[33]
			10	[34]
	617 cycles (1100–25°C)	1.84–1.90	8.83–10.05	[35]
Replacement of the larger La ion by the smaller and heavier Yb ion leads to lower thermal conductivity through greater dissipation of 'hot' phonons				[36]
				[37]
5.292–4.928				[38]
In the $Sm_2Zr_2O_7 + Al_2O_3 \leftrightarrows m\text{-}ZrO_2 + SmAlO_3$ reaction, the coating is delaminated because of different thermal expansion coefficients of the existing phases				[39]
7.295 6.586				[40]
	3100 cycles; YSZ – 2400 cycles (1100–25°C)			[41]
The phase decomposes above 900°C				[42]
				[43]
6.03–6.37				[44]
			8.9 12.1 11.7 10.7 9.6 12.3	[45]

Material	Deposition/ production technique	Thermal conductivity, $W \cdot m^{-1} \cdot K^{-1}$	Thermal expansion coefficient α, $10^{-6} \cdot K^{-1}$	Young's modulus E, GPa
$Gd_2Zr_2O_7$	APS	1.4–0.6 (800–25°C)		
$Nd_2Zr_2O_7(N_2Z)$ N_2Z/YSZ	APS	0.55–0.8 0.55–0.75 (500–1000°C)		
$La_2(Zr_{0.7}Ce_{0.3})_2O_7/YSZ$ $MAl_{11}O_{19}$(Mg, Mn, Fe)	EB-PVD			
$(La,Gd)_2Ce_2O_7$	Chemical	0.96–1.96 (200–800°C)	11–12	
$(Sm,Dy)_2Ce_2O_7$	Ceramic	1.38–1.69 (1000°C)	11.02–11.24	
$La_2Zr_2O_7$ $Gd_2Zr_2O_7$ $La_2Ce_2O_7$ $La_2(Zr,Ce)_2O_7$	Chemical			
$(Gd_{0.9}Yb_{0.1})_2Zr_2O_7/8YSZ$	EB-PVD, gradient coating		11.8	
$(La,Yb,Er)_2Zr_2O_7$	Ceramic	1.22–1.32	9.54–9.78	180
$(Gd,Yb)_2Zr_2O_7$ $(Gd,Yb)_2Zr_2O_7/YSZ$ $Gd_2Zr_2O_7$	Ceramic, EB-PVD	0.8–1.1 (25–1000°C) ~1.18	11.8–13	266
$(La,Eu)_2Zr_2O_7$	APS			
$(Ca_2Nb_2O_7)_x(Gd_2Zr_2O_7)_{1-x}$	Ceramic	1.6–2.05		230 $x = 0.9$

There has been significant progress in the fundamental understanding of the TBC deposition processes in the recent years. The mechanisms responsible for various types of porosity in the EB-PVD coatings [114–116] reveal several ways for interaction between the front growth and vapor beams. Shadowing of the incident vapor is even more important as it plays a decisive role in the in-plane and out-of-plane textures of the columnar coatings [117] and in the change of microstructures.

The latter results from local changes in the direction of vapor flows formed under the influence of surface geometric features [117, 118]. The latest developments in research techniques [119] open new prospects for predicting the properties and optimizing the coating deposition processes through required quantitative data on such complex microstructures.

In addition to the above, a series of other TBC deposition techniques have been developed. They include metalorganic chemical vapor deposition [120]. In this technique, cheaper metalorganic compounds react with oxygen-containing compounds (O_2, H_2O, H_2/CO_2) at relatively low temperatures (850−1000°C) to form YSZ coatings. The drawback is carbon deposition and formation of zirconium carbides, affecting the coating properties. The glassy coating technique [121] involves the atomization of powders, e.g. ZrO_2 (3 wt.% Y_2O_3), in exceptionally thermally resistant aluminum borosilicate glass $AO−B_2O−C_2O_3−SiO_2$ (A = Ca, Mg, Ba; B = Na, K; C = Al, B).

Table 2 finished

Specific weight, g/cm^3	Thermal stability	K_{Ic} MPa·m$^{0.5}$	Vickers hardness, GPa	Ref.
				[46]
				[47]
	2507 cycles (1200–25°C) 27% higher than for YSZ	Low sinterability		[48]
				[49]
				[50]
5.1–5.9 6.1–6.9 6.3–6.4 5.6–5.7	La$_2$Zr$_2$O$_7$ and Gd$_2$Zr$_2$O$_7$ are the most thermally stable phases			[51]
		1346 cycles (1350–25°C)		[52]
6.036–6.147				[53]
		3700 cycles (25–1350°C)	~8.8	[54]
	32 cycles (1250–22°C)			[55]
		1.5–3	8	[56]

The sol–gel route has advantages such as lower cost, greater flexibility, and recoverability of damaged coatings [122]. This technique is also promising for producing low-temperature film sensors to monitor human health [123].

A new plasma spraying technique has been developed to reduce oxidation in the spraying process. It involves low-pressure or vacuum plasma spraying and promotes rapid deposition of coatings [124]. In particular, this technique is an additional viable alternative to the APS and EB-PVD processes.

Thermal Barrier Coating Mechanical Properties. Besides the high-temperature thermal properties, mechanical properties are very important for TBC applications, such as Young's modulus, hardness, strength, and fracture toughness. Under the influence of high-temperature gases, hot erosion plays a decisive role in the life of coatings [125, 126]. In addition, TBCs are subjected to severe thermal stresses associated with heating and cooling. Hence, the coatings should withstand high stresses without fracture, which requires high crack resistance and yield strength. The coatings should possess high fracture toughness to be resistant to shock and erosion and to delamination as well [2, 127].

To characterize thermal shock resistance, the critical thermal shock resistance factor R is used, which is determined as:
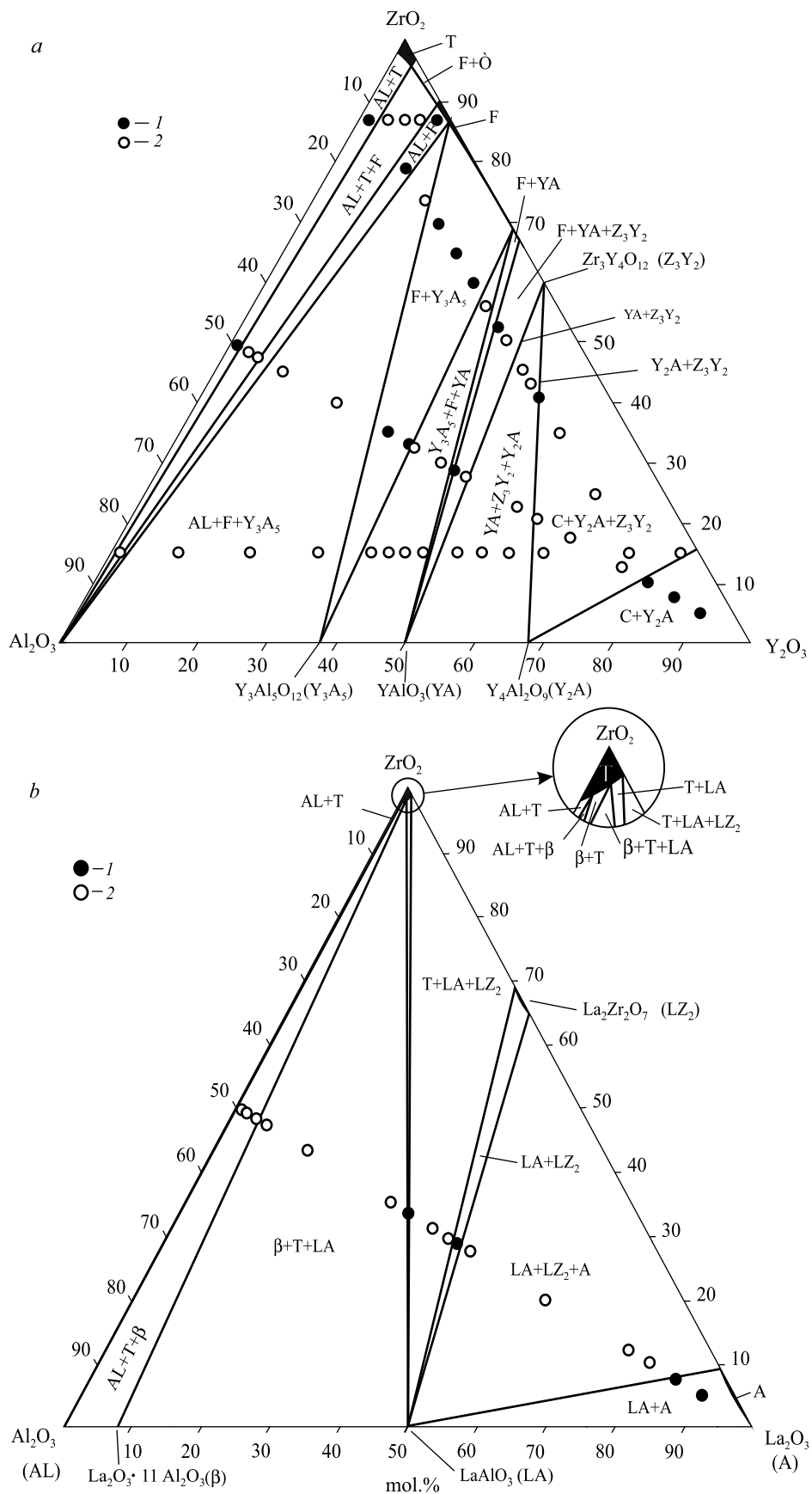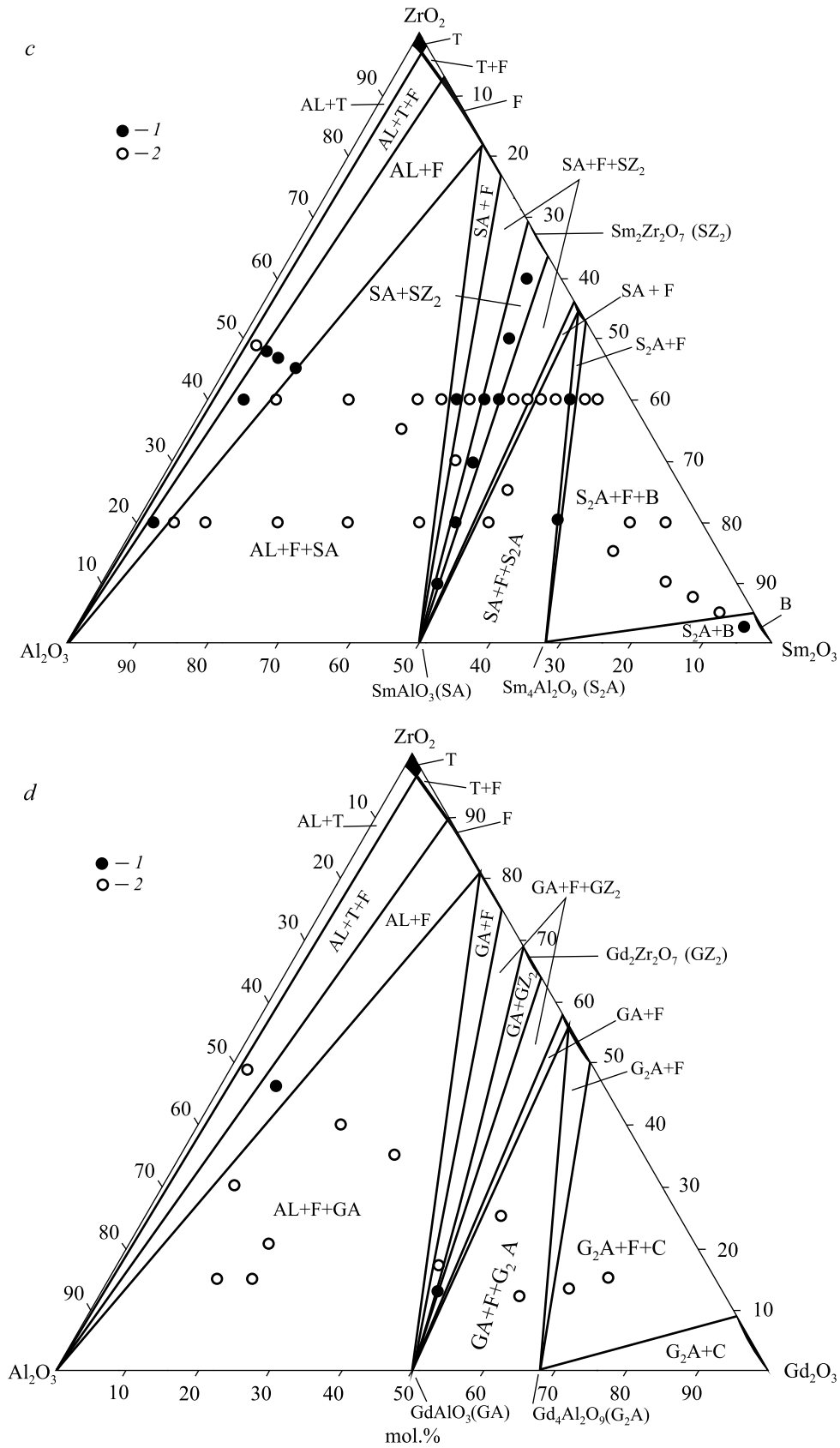
$$R = \sigma_f(1 - \mu)/E\alpha, \tag{1}$$

Fig. 2. Isothermal sections of the Al_2O_3–ZrO_2–Y_2O_3 (*a*) and Al_2O_3–ZrO_2–La_2O_3 (*b*) phase diagrams at 1250°C: *1*) two-phase samples and *2*) three-phase samples

Fig. 2 finished. Isothermal sections of the Al_2O_3–ZrO_2–Sm_2O_3 (*c*) and Al_2O_3–ZrO_2–Gd_2O_3 (*d*) phase diagrams at 1250°C: *1*) two-phase samples and *2*) three-phase samples

TABLE 3. Some Materials Promising as TBCs

Material	Deposition / production method	Thermal conductivity, $W \cdot m^{-1} \cdot K^{-1}$	Thermal expansion coefficient α, $10^{-6} \cdot K^{-1}$	Young's modulus E, GPa
$LaMgAl_{11}O_{19}$	APS / chemical	1.2–2.0 (300–1200°C)		
$HfO_2(7\,Y_2O_3)$	EB-PVD	6–9 (200–1400°C)		
$SrZrO_3$	APS / ceramic	~ 2.1 (600–1000°C)	~11	170
$YSZ + 5\%\ Al_2O_3$	APS			103.44–138.70
$LnPO_4$ (Ln = La, Ce, Nd, Sm, Eu, Gd)	Chemical	3.5–1.3 (25–1000°C)		130–170
$LnMgAl_{11}O_{19}$ (Ln = La, Nd, Sm, Gd, Sr)	APS			
$LaAl_{11}O_{18}$	Chemical	1.5 (500–1100°C)		
$LaMgAl_{11}O_{18}$:Dy	Chemical	2.52–2.89 (1200°C)	7.5–8 (500–1200°C)	
$Ln_2SrAl_2O_7$ Ln = La, Nd, Sm, Eu, Gd, Dy	Ceramic	3 1.6 2.5 2.42 2.4 2.3		166.4 186.0 252.3 240.0 257.9 230.4
YSZ/Al_2O_3	Ceramic			
13 mol.% Al_2O_3–8YSZ	APS			
Mullite	APS	1.4		
$LaTi_2Al_9O_{19}$/YSZ	APS			
$LaMgAl_{11}O_{19}$	APS			295
Ti_2AlC	High-speed deposition with a soldering iron in air	4.0		
Al_2O_3–ZrO_2	Slip casting	Not lower than YSZ		
$LaMgAl_{11}O_{19}$/YbAG		2.6–3.9 (25–1200°C)	7–8 (400–1200°C)	
$InFeSnO_4$	Ceramic	2.86–1.36 (25–1200°C)	~11.7 (1200°C)	
$LaTi_2Al_9O_{19}$	APS	1.0–1.3 (300–1500°C)	8.0–11.2 (200–1400°C)	99.6
HfO_2(7.5 mol.% Y_2O_3)	High-frequency magnetron sputtering	0.89–1.3 (25–500°C)		
$La_2Ce_2O_7$	APS	LC reacts with Al_2O_3 and, hence, two-layer YSZ coating is recommended. The properties of the two-layer coating are worse than those of LC		

Specific weight, 10^3 kg/m^3	Thermal stability	K_{Ic}, MPa · m$^{0.5}$	Vickers hardness, GPa	Ref.
				[61]
	100°C higher than for YSZ			[12]
	1514 cycles (25–1250°C)	1.5	9.2	[62]
			7.55–11.35	[63]
				[64]
	1240–5560 thermal cycles			[65]
				[66]
				[67]
5.711 5.914 6.082 6.133 6.343 6.508				[68]
Al$_2$O$_3$ increases thermal conductivity				[69]
YSZ sintering is slowed down				[70]
Upper operating temperature limit is 1000°C				[71]
2000 cycles 25–1300°C		1–3		[72]
4.285			6–8 (200–1400°C)	[73]
The phase decomposes above 900°C				[74]
				[75]
				[76]
				[77]
	1300 (25–1300°C, 700 h)	0.9–1.7	~7	[72]
				[78]
				[79]

Material	Deposition/production method	Thermal conductivity, $W \cdot m^{-1} \cdot K^{-1}$	Thermal expansion coefficient α, $10^{-6} \cdot K^{-1}$	Young's modulus E, GPa
YbAG	First principles calculations	1.22 (1000 K)	7.5	257
YAM	Ceramic	1.81 (1000°C)	8.91 (300–1200°C)	
$(Ca_2Nb_2O_7)_x$ $(Gd_2Zr_2O_7)_{1-x}$	Ceramic	1.6 (200–1000°C)		230 $x = 0.5$
$La_2(Zr_{0.7}Ce_{0.3})O_7/YSZ$	EB-PVD			
$ZrO_2–Ta_2O_5–Yb_2O_5$	EB-PVD			
$Yb_3Al_5O_{12}$	Ceramic		8.22	282
$ThO_2–8YSZ$	Chemical	1.95 (1000°C)	10.94–10.47	213–250
$Ce_{1-x}Sm_xO_{2-x/2}$	Sol–gel	1.62–2.02		

where σ_f is the bending strength, μ is Poisson's ratio, E is Young's modulus, and α is the thermal expansion coefficient. The higher R, the higher the thermal shock resistance. In terms of R, it should be noted that the TBC should have maximum bending strength σ_f and minimum Poisson's ratio, Young's modulus, and thermal expansion coefficient [82].

To assess the mechanical properties of new TBC materials, they should be compared to those for the standard YSZ coating. The average values of the mechanical properties of the YSZ coating are provided below [82]:

Bending strength, σ_f. . . . . 120 MPa
Compressive strength, σ_c. . . . . 270–700 MPa
Fracture toughness, K_{Ic}. . . . . 1.7–2.0 MPa $\cdot$ m$^{0.5}$
Vickers hardness, HV. . . . . 14 GPa
Brittleness index, M. . . . . 7 μm$^{-0.5}$
Fracture resistance, D_t. . . . . 0.25 M$^{0.5}$

Analysis of the literature (Tables 2 and 3) indicates that the mechanical properties of new TBC promising materials have not been fully determined. This stimulates appropriate research of the sintered materials and associated coatings.

Control of the Thermal Barrier Coating Microstructure. After the material with relatively low thermal conductivity has been chosen and its inactivity relative to Al_2O_3 and adequate mechanical properties have been ascertained, the thermal conductivity of the TBC can be reduced by controlling its microstructure. First of all, this can be done by selecting the appropriate spraying method. Here, EB-PVD deserves the first place. To optimize the microstructure of coatings deposited by this technique, one should understand the microstructural features and their contribution to thermal isolation and changes in operation.

Figure 4 shows the main types of porosity for the EB-PVD YSZ coating [13]. The gaps between columns denoted as type 1 (Fig. 4) arise from vapor condensation and macroscopic shadowing caused by the curvature of column tips resulting from rotation of parts being sprayed. Since shadowing primarily acts along the vapor incidence plane; the gaps are much wider in the direction parallel to the rotation axis than in the perpendicular direction [117, 128–131].

Table 3 finished

Specific weight, 10^3 kg/m^3	Thermal stability	K_{Ic}, MPa · m$^{0.5}$	Vickers hardness, GPa	Ref.
6.67				[58]
Lower than that of YSZ				[57]
		1.5–3	8	[56]
	6734 thermal cycles (373–1373 K)			[80]
Increased stability of the t' phase. The tetragonal YbNa(Zr)O$_4$ phase precipitates at 1850°C				[81]
		2.88	10.7	[82]
				[83]
				[84]

The round and elongated pores (type 2) result from rotation as well. They are located in layers from the column edge to the center almost in parallel with the substrate surface, i.e., parallel to each column tip in the growth process. Each layer corresponds to one rotation. Pores of this type are apparently closed.

The latter microstructural feature, called feather-like one (type 3 in Fig. 4), evolves from shadows cast by steps on the column tip faces [117]. Since the {111} planes are favored in terms of energy in the construction of faces at column tips, multiple growth steps appear when the tip is distorted because of macroscopic shadowing. In further growth, these steps in turn serve as shadowing centers. This leads to the maximum open porosity oriented at an angle of about 45° to the main column axis. Open voids 200−250 nm in size appear in pore feathers (type 3) with a typical width-to-length 1 : 10 ratio [132, 133]. All three types of porosity generate a large specific surface area (4−6 m^2/g) for the EB-PVD YSZ coatings.

Reduction in the thermal conductivity of such coatings can be controlled through intracolumnar pores of types 2 and 3, while intercolumnar pores (type 1) do not so effectively influence the thermal conductivity. The pore size, distribution, concentration, and morphology are important factors that characterize intracolumnar porosity. The microstructure of the EB-PVD coatings depend on process parameters such as spraying temperature, rotation velocity, chamber gas pressure, vapor flow direction, shadowing, etc. [13].

The microstructure rapidly changes in high-temperature TBC performance. Intercolumnar sintering of type 1 pores increases the ceramics' Young's modulus through the formation of contact points between the columns, leading to increase in stresses in the coating in the performance process [130, 131]. Additional elastic energy accumulated by the ceramics provides further driving force for crack origination and propagation and causes delamination of the coating, decreasing its resistance. This occurs when operating temperature exceeds 1200–1300°C, but microstructural changes are observed even at 900°C. These changes increase the thermal conductivity. For EB-PVD TBCs, this increase depends on temperature, but is no more than 20% at a certain temperature mode [134, 135], being much lower than for plasma-sprayed TBCs.

Coating sintering includes several mechanisms [128, 129, 131, 136, 137]:

- decrease in the internal free surface energy, mainly through the transformation of feathers into a linear row of coarser closed pores, forming a rounded smooth column surface;
- additional growth of type 2 and type 3 pores, accompanied by change in their percentage;
- formation of throats at column contact points near type 1 pores resulting from sintering.
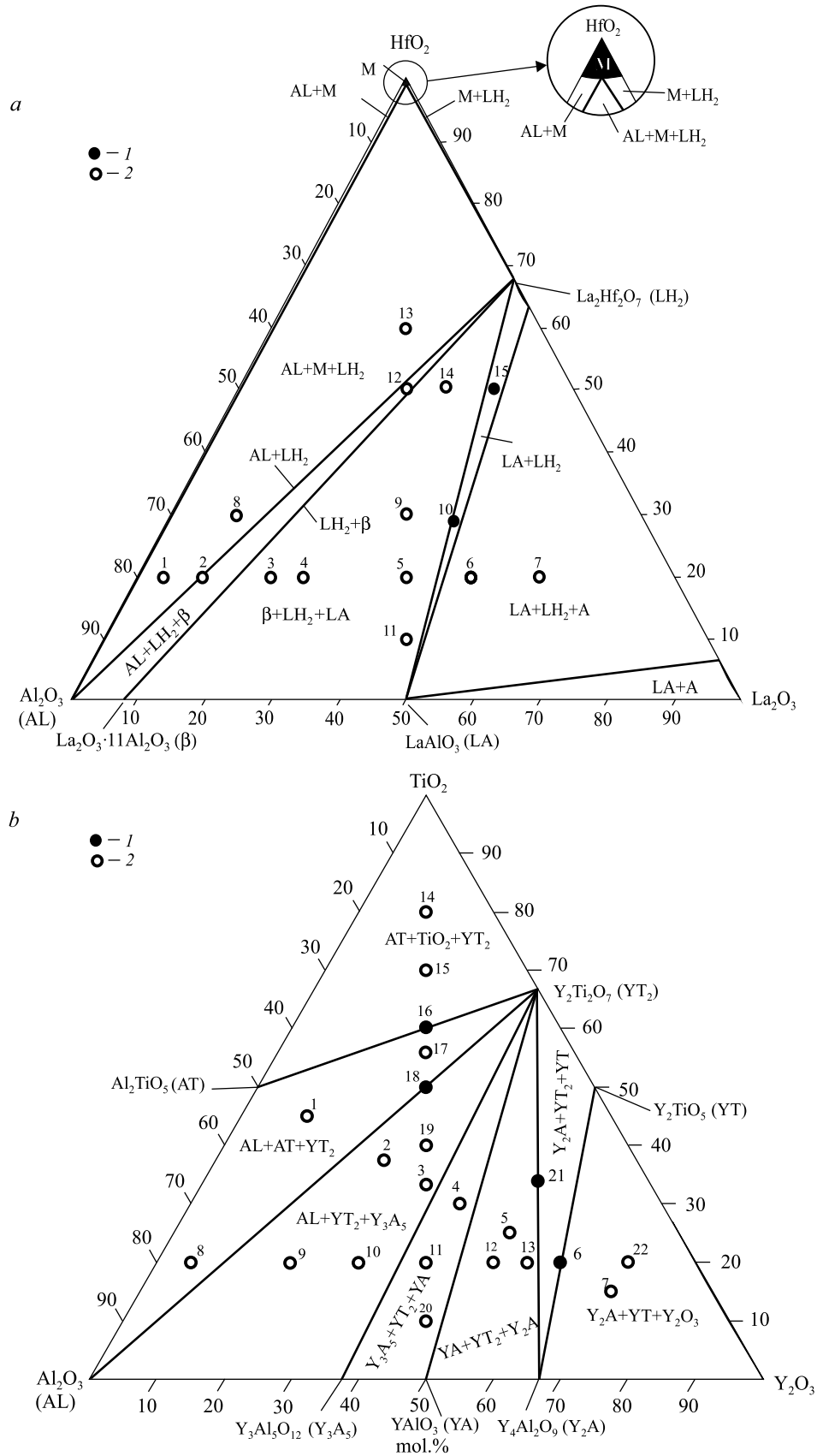
Fig. 3. Isothermal sections of the Al_2O_3–HfO_2–Y_2O_3 (*a*) and Al_2O_3–TiO_2–Y_2O_3 (*b*) phase diagrams at 1250°C: *1*) two-phase samples and *2*) three-phase samples
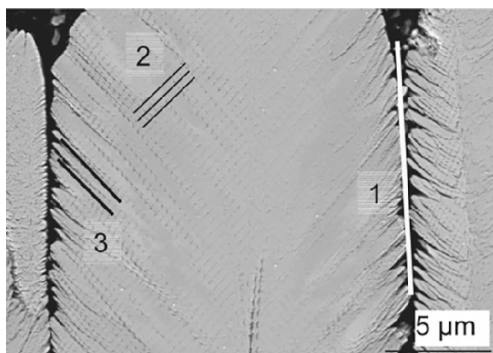
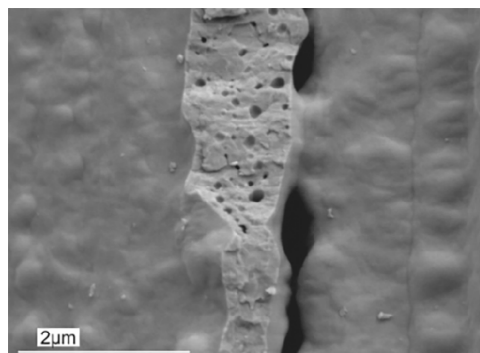Fig. 4. Three types of pores in as-deposited EB-PVD YSZ coating [13] | Fig. 5. Microstructure of the EB-PVD coating after nine-time annealing for 100 h at 1100°C [13]

An example of microstructural change is shown in Fig. 5 [13]. Although the overall coating density changes insignificantly, the pore specific surface area significantly decreases above 900°C, which indicates that coarse pores are generated through fine pores (for example, <10 nm). Considering only pores larger than 1 μm, which can be determined by microcomputed tomography, it was established that porosity abruptly decreased at temperatures below 1100°C in the coating lower part because of a large number of fine columns, while the percentage of pores coarser than 1 μm increases in the upper coating part. To retain low thermal conductivity, significant sintering resistance is required for the coating to perform at high temperatures for a long time.

The phase stability of ceramic coatings is one of the requirements imposed on modern TBCs that perform at operating temperatures above 1200°C. Although the published data do not always agree, most research efforts demonstrate that the metastable t' phase rapidly decomposes into the stable monoclinic and cubic phases [128, 136, 138]. Depending on the cooling conditions and, probably, on the sample production techniques (free spraying or spraying onto metal or sapphire substrates, which control the stresses in TBCs), the monoclinic phase may be present at room temperature. A small amount of the monoclinic phase was found on real blades, especially on concave surfaces, already after 350 h at 1100°C and after engine tests [139]. The formation of the monoclinic phase is an important factor since phase transition t ⇆ m is associated with volume changes up to 5%, inducing substantial loads on the ceramic coating. There are data confirming that a significant amount of the monoclinic phase in as-deposited EB-PVD coatings may be acceptable [140].

The microstructure and properties of TBCs can be controlled by variation in their deposition conditions. At high chamber pressures and low substrate temperatures, the EB-PVD coatings have low density, characterized by large gaps between the columns and column diameters increasing with coating thickness growth [141].

The lower the substrate temperature, the lower the capability of the condensed atoms to diffuse into stable lattice positions. This leads to the formation of perturbed and imperfect low-density microstructure. The dependence between the density and thermal conductivity is linear and allows about 15% decrease in the thermal conductivity. Greater decrease in the thermal conductivity and improvement in the life of the coatings were identified for TBCs deposited at increased pressures (to 0.15 Pa) using a mixture of oxygen and inert gas [101]. The formation of inclined columns is an inherent capability of such coatings. Any deviation of vapor incidence on the substrate from perpendicular direction leads to column inclination regardless of the cause. The deviation may be caused by slope of the sample rotation axes [142], failure to place the part strictly above the evaporating bath, or slope of the substrate plate in case of stationary spraying [143]. The knowledge of these features was used to produce the so-called zigzag or fir-tree structures, promoting a significant decrease (to 40%) in the thermal conductivity [144]. Figure 6 shows an example of the microstructure formed in this way [13]. The main issue with the sloped columnar structures is that they are sensitive to erosion. The greater the column slope, the lower the erosion resistance [144–146]. Such microstructures were acquired through variation in the rotation velocity and vapor incidence angle. The expected decrease in thermal conductivity reached 20%. The same zigzag microstructures were successfully obtained by directed electron-beam spraying [147, 148].
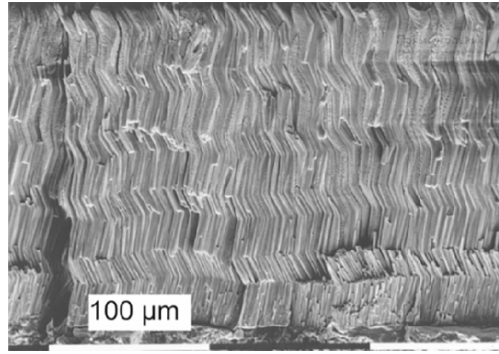
Fig. 6. Zigzag structure of the EB-PVD coating [13]

The microstructure of the EB-PVD coatings, especially porosity of type 2, can be easily changed by varying the sample rotation velocity [149]. There is no unique correlation between the rotation velocity and thermal conductivity [145], though it can be assumed that the number of type 2 pores between the layers will increase and, hence, the thermal conductivity will decrease at a high rotation velocity. The knob-like structure acquired by the columns through simultaneous change in the rotation velocity and spraying temperature in the EB-PVD process allowed TBCs with exceptionally low Young's modulus and low tendency to sintering to be produced [129]. A large number of small columns forms near the substrate surface; most of them degenerate in the further growth process and only several columns reached large sizes. The microstructure of this area (commonly smaller than 20–30 µm) has a large number of boundaries on the thermal flow pathway. Therefore, the thermal conductivity in this area is much lower [145, 150]. The thinnest coating (52 µm) showed 35% lower thermal conductivity than the coating 350 µm in thickness. This dependence of the thermal conductivity of EB-PVD coatings on their thickness should be taken into account in comparing the isolation properties of new coatings.

To obtain similar structures across the coating thickness, interrupted spraying method should be applied. This can be achieved by successive introduction of the sample holder into and its removal from the chamber or periodic blocking of vapor flows. The thermal conductivity of the coatings deposited in this way only slightly decreases, though microstructural changes are observed exactly with this technique and result from significant temperature fluctuations [151, 152]. This leads to a 20% decrease in the thermal conductivity as a maximum. High-temperature holding to 1316°C produces a layered porous structure with better thermal properties. Although the effectiveness of this technique has been proven, the producers are still reluctant to use it commercially because of frequent annealing processes, reducing the cost effectiveness.

The coating base microstructure was changed by periodic injection of a polluting environment into the spraying chamber to repeatedly generate a ceramic layer, thus decreasing its thermal conductivity [104]. This method changes the density of individual layers and ensures up to 37–45% decrease in the thermal conductivity at low temperatures [7, 150].
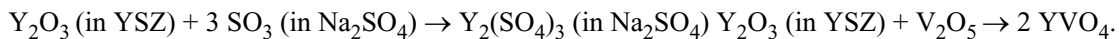
The long-term stability of any coating is ensured by its high erosion properties. In this regard, it was proposed that the outer coating was deposited onto the type 3 feathers by impregnation [153, 154]. This allowed the low thermal conductivity to be retained and Young's modulus to be decreased to a smaller extent under thermal load. The TBC ceramic body remains unchanged. Sol–gel impregnation with titanium dioxide showed that the success of this approach depended on the capabilities of nanotechnologies. Hence, further research efforts are needed to fully use the capabilities of this method.

CORROSION RESISTANCE OF THERMAL BARRIER COATINGS

Fuel Combustion Products. Two types of corrosion are considered for modern TBCs: corrosion of the upper ceramic coating (resulting from the reaction of V_2O_3 and Na_2SO_4 contained in the combustion products of low-quality fuel with CMAS glass (calcium–magnesium–aluminum–silicate) absorbed into the engine with air) and oxidation of the blade material in the performance process.

In addition, small SiO_2 admixtures (even to 1 wt.%) in the YSZ coating adversely affect its life [4]. In dense zirconia-based ceramics, ZrO_2 segregates mostly to grain boundaries collecting at the so-called ternary points. Its presence at grain boundaries changes their size and shape and can dissolve Y_2O_3 present in near-boundary YSZ grains. This leads to local destabilization of these grains. Silicon dioxide can increase the superplasticity of ZrO_2 polycrystals and, as a result, significantly increase the sintering rate and decrease electrical conductivity. This may also lead to higher creep rate, which was the case for silicon-containing ceramics [155]. On the other hand, silicates have much lower oxygen conductivity than YSZ and, thus, the thick silicate film on the bond coating can serve as an oxygen barrier and improve oxidation resistance of the coating [156].

Admixtures (mainly Na and V) contained in low-quality fuel (e.g., in petroleum coke) form salts Na_2SO_4 and V_2O_5 on the turbine blades. The mechanism whereby these coatings fail involves the interaction of these compounds with Y_2O_3 (stabilizer for ZrO_2) to form YVO_4. The stabilizer is washed from the coating that fails in destructive phase transformation T-ZrO_2 ⇆ M-ZrO_2 because of a 3–5% volume increase [25, 156, 158–160]. The resultant reactions can be written as follows [26]:

$$Y_2O_3 \text{ (in YSZ)} + 3 SO_3 \text{ (in } Na_2SO_4) \rightarrow Y_2(SO_4)_3 \text{ (in } Na_2SO_4) \text{ } Y_2O_3 \text{ (in YSZ)} + V_2O_5 \rightarrow 2 \text{ } YVO_4.$$

A number of methods was proposed to improve TBC high-temperature corrosion resistance using the most stable stabilizers, such as In_2O_3, Sc_2O_3, CeO_2, etc. [158, 161, 162], deposition of the densest upper alumina layer on the YSZ surface [163], and laser glazing and repeated melting to produce a dense porousless coating that prevents the penetration of salts [164].

The papers [9, 165, 166] show that the life of the YSZ coating is quite long in a Na_2SO_4 environment, but short in V_2O_5. The $La_2Zr_2O_7$ coating demonstrates good resistance to hot corrosion of V_2O_5, but not to Na_2SO_4. Both types of coatings show limited high-temperature corrosion resistance in a Na_2SO_4 and V_2O_5 mixture.

In case of the YSZ + $Gd_2Zr_2O_7$ coating, the molten Na_2SO_4 + V_2O_5 mixture reacts with the $Gd_2Zr_2O_7$ phase to form $GdVO_4$ and M-ZrO_2 [167]. The dependence of the degradation rate on the corrosion layer thickness and general coating condition after high-temperature corrosion have led to the conclusions that the $Gd_2Zr_2O_7$ coatings demonstrate higher corrosion resistance at 1050°C than the YSZ coating [168].

It is established [169] that P_2O_5 reacts with the YSZ coatings produced by APS with the formation of zirconium pyrophosphate (ZrP_2O_7) at all experimental temperatures. At 200–1200°C, molten P_2O_5 reacts with solid YSZ to form ZrP_2O_7, which decreases the amount of ZrO_2 in YSZ (i.e., t'-YSZ enriches in Y_2O_3), promoting the cubic ZrO_2 phase of fluorite type. After laser treatment, dense layers of different compositions can be produced on the 8YSZ APS coatings. In contact with the V_2O_5 + Na_2SO_4 corrosive mixtures for 100 h at 1173 K, the 8YSZ TBC with an Al_2O_3 layer showed good corrosion behavior at high temperatures and, hence, longer service life [170].

CMAS Attack. Increase in the operating temperature of engines also creates new issues for the materials for ceramic TBCs, such as degradation of 7YSZ TBCs resulting from the melting of silicate deposits [157, 171–174] caused by the adsorption of fine particles from the environment (sand [157], volcanic ash [175]). In view of the major components of borosilicate glass, this phenomenon is commonly called the CMAS attack. This in turn affects the engines that perform at temperatures higher than conventional ones. In case of ground-based power generators, it is difficult to filter out the finest particles transferred together with input air by alternative fuel, such as, for example, syngas [176]. Therefore, the mitigation of CMAS attack becomes an additional important requirement for future TBCs.

The researchers paid great attention to preventing the CMAS effect on TBC stability [171, 177]. All results can be divided into two areas: (i) using a sealant or suppressing the wetting of the outer coating layer [178] and (ii) introducing a sacrificial layer or crystalline Al_2O_3 particles into the 7YSZ coating [178, 179]. The first approach suffers from cracking/erosion of the outer layers in thermal cycling and operation, while the logical justification for the other is to inhibit the propagation of the CMAS front using Al_2O_3. This approach is limited by stresses induced by different thermal expansion coefficients of the 7YSZ coating and the other phase (Al_2O_3) and by increase in the total thermal conductivity of the coatings.
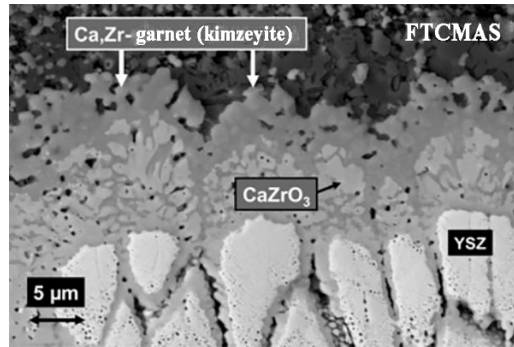
Fig. 7. Double CaZrO$_3$/kimzeyite layer in the FTCMAS/YSZ reaction area in the TBC upper part

(backscattered electron image) [180]

According to [180], the larger the REM cations, the faster the solidification of the CMAS silicate melt; the relative effectiveness increases with higher REM oxide content of zirconate or hafnate coating materials containing Yb$_2$O$_3$, Gd$_2$O$_3$, or La$_2$O$_3$.

To be effective against the CMAS attack, the coating ceramics should actively interact with molten glass for rapid solidification [177]. The formation of Y$_2$Zr$_2$O$_7$ seems to be optimum for suppressing the penetration of molten CMAS almost completely.

The microstructure of the reaction area (Fig. 7) for the YSZ coating and FTCMAS (F and T are Fe$_2$O$_3$ and TiO$_2$) and the compatibility of phases determined with additional sintering experiments show that the corrosion processes occur in two stages [181]. The first stage involves a silicon-free, calcium source; it is most probably CaSO$_4$ from the vapor phase that form a thin CaZrO$_3$ layer on the upper coating. The second stage involving highly active Fe, Ti, and Si and being unfavorable for the formation of CaZrO$_3$ stabilizes the kimzeyite phase (kimzeyite is a mineral with empirical formula Ca$_3$(Zr, Ti, Fe)$_2$(Al, Fe, Si)$_3$O$_{12}$) with garnet structure.

The double CaZrO$_3$/kimzeyite layer can be used as a sensor to evaluate the effective operating temperatures for the YSZ-coated turbine blade. This layer provides an effective diffusion barrier for CMAS components on the coating hot area.

The wide homogeneity range makes the kimzeyite garnet structure an effective absorber of FTCMAS components, compensating for the chemical gradient and reducing the driving force for dissolving the YSZ coating. If the maximum temperature of the turbine blade surface is no more than the kimzeyite melting point (~1290°C) [182], the coating can perform smoothly for a long time.

Volcanic Ash. Studying the effect of airborne volcanic ash on the performance of the EB-PVD YSZ coating of high-pressure turbine aerodynamic surfaces [183] showed that it was different from that of CMAS. The EB-PVD YSZ coating is completely wetted and partially impregnated with volcanic ash at 1100°C, which is 100−150°C lower than the CMAS onset infiltration temperature. At 1200°C, besides the residual plagioclase and hematite phases, the upper glazed layer of volcanic ash penetrates deep into the coating. Since volcanic ash acts as an effective Y$_2$O$_3$ solvent above 1000°C, yttria content of the YSZ decreases, but complete YSZ destabilization, i.e., transformation into the monoclinic phase, is not observed. Instead, the ZrSiO$_4$ phase appears at 1200°C. For noticeable interaction of the YSZ coating with volcanic ash, a greater amount of the latter and longer thermal load are needed. The coating impregnated with volcanic ash is expected to have higher thermal stresses in thermal cycling, which will reduce the coating service life. The change in the microstructure (resorption and coalescence of pores) may worsen the thermal insulation characteristics, as established for the CMAS [184]. In addition, it is impossible to control the interaction of impregnated volcanic ash and Al$_2$O$_3$ at the YSZ/bond coating interface. Relatively low softening temperature (1100°C) and viscous volcanic ash flow can also cause serious problems for blade cooling holes. It should be emphasized that ash from different volcanic provinces has different chemical and phase compositions and, therefore, can interact with YSZ TBC in different ways.

Various researchers have found that gadolinium zirconate $Gd_2Zr_2O_7$ is resistant to the action of molten CMAS [185–188]. It is shown in [176] that the $Gd_2Zr_2O_7$ APS coating is extremely effective against damage by molten bulk deposits of fly ash. The results demonstrate that the volatile ash of brown coal, present as particulate impurities in syngas, penetrates across the entire thickness (200 μm) of the coating and destroys it in contact with conventional 7YSZ APS coatings at 1200°C. Nevertheless, the $Gd_2Zr_2O_7$ APS coatings have high stability under the same conditions, since the molten volatile ash impregnates only 25% of the coating thickness. The TBC damage reduces through the formation of a stable impermeable crystalline layer at the boundary between the TBC and molten airborne ash. The mechanism whereby the molten airborne lignite ash attacks the 7YSZ APS coating is identical to the action of CMAS sand and volcanic ash.

CONCLUSIONS AND PROSPECTS FOR DEVELOPMENT

Thermal barrier coatings have become an integral part of turbine designs, which should be more efficient and productive and generate less emissions and noise. This will be even more important in meeting the growing energy and transport needs of society, as long as large-scale renewable energy production (solar energy, wind, etc.) will become more economically viable.

The future of parts with directionally solidified eutectics will also depend on TBCs. The thermal barrier coatings have evolved from simple insulating layers to complex structures. However, the turbine designers have a questionable attitude toward TBC because of the unacceptable scatter of laboratory and performance characteristics of the engines, even with the YSZ base coating, for various reasons that are mainly related to technology and damage from microfibers in the turbine operating environment. This requires that the turbine be operated in the lowest part of this scattered range of properties. Therefore, it is needed to narrow the range of performances to increase the TBC efficiency [189].

The complexity of interaction between the four main layers and materials in the TBC (upper ceramic coating, thermally grown oxide, bond metal coating, base superalloy) and their evolution with time and temperature require synergetic progress in all areas for reliable operation of TBCs at even higher temperatures in the future.

There are three main problems. The first is to increase the reproducibility in depositing the coatings. The second is to simulate more fully the evolution and destruction of the coating during operation, as well as to obtain a more detailed description of its properties, especially at high temperatures. The third major problem is to solve new issues that arise at higher temperatures. In particular, this includes radiation transfer of heat through the TBC. New approaches will be needed to reflect and/or dissipate radiation and prevent exposure of metal parts [171].

High-quality thermal barrier coatings withstand a very high thermal flux when tested in a plasma torch. These observations suggest that the thermal flow of the gas turbine engine is not a major factor in the deterioration of the coating quality [1].

The use of TBCs ensures the necessary thermal protection against hot gases in turbines and engines and, therefore, is the main way to reduce surface temperature of the parts. However, there are problems in operation in harsh environments at high temperatures. This includes corrosion, oxidation, erosion, surface damage, sintering, and phase transformations. The YSZ coatings fail because of stresses induced by bulk changes that accompany phase transformations [160].

The TBC in operation is a dynamic system. The constituent parts of this system (upper layer, thermally grown oxide, bond coating, and base superalloy) undergo continuous changes in the composition, microstructure, and crystalline phases throughout the service life. This leads to changes in the mechanical and physical properties of TBCs at different stages of their operation [3].

The temperature in the bond coating can still be expected to be the most important factor, though the effect of temperature gradients on phase transformations, surface sintering and compaction, compensation of strain at the interfaces, as well as oxidation and mechanical properties of the bond coating will also play an important role [1].

The bond coating influences the slow formation of thermally grown oxide, service life, replacement of platinum group metals, and reduction in interdiffusion. There is still a need to minimize the use of expensive elements (Pt, Re, Ta, and Ru). The sufficient REM amounts are also a concern for producers [189]. The maximum

temperature of the bond coating will continue to be limited by temperature of the blade alloy because of the minimum temperature gradient between the bond coating and substrate. The predictions of service life and tests of oxidation and hot corrosion resistance, simulating the engine behavior, will be ongoing. The search for effective diffusion barriers will continue as well.

Moreover, a thin layer (0.05–0.1 μm) consisting of zirconium and yttrium oxide particles scattered in the matrix of thermally grown oxide is formed between the upper layer of the YSZ coating and oxide during preheating and application of the upper layer by EB-PVD [190]. The mechanism whereby this 'mixed area' influences the TBC/oxide adhesion needs to be further examined and verified.

Efforts are ongoing to achieve 'high confidence' for TBC. High confidence requires eliminating the instabilities in the deposition processes, ensuring the quality and effectiveness over time, and providing for long and predictable life of the TBCs.

The APS and EB-PVD techniques continue to be the most versatile and contribute to the rapid deposition process. The former provides higher efficiency of isolation and the other ensures longer life [3] and is statistically more reliable [191].

The technological developments in the field of advanced vacuum plasma spraying have led to innovative changes in existing processes and to a number of new processes, such as plasma spraying of suspensions, method of dense vertical cracks, and directed vapor deposition [189].

The new generation of ceramic TBCs with lower thermal conductivity includes several interesting zirconates, such as $Gd_2Zr_2O_7$, $Sm_2Zr_2O_7$, $Nd_2Zr_2O_7$, $La_2Zr_2O_7$, and $Dy_2Zr_2O_7$ and compounds BaY_2O_4, $LaTi_2Al_9O_{10}$, SrY_2O_4, and $Sr(Zr_{0.9}Yb_{0.1})O_{2.95}$ [192]. However, there are concerns relating to potential destructive interactions between the TBC and grown oxide, as the TBC–oxide integrity is vital for system service life [6]. So far, many of the newly developed EB-PVD TBCs have been put into operation or ground tests only with the basic standard ceramic YSZ layer.

Rear earth metal oxides are promising for TBCs due to their low thermal conductivity, high thermal expansion coefficient, and chemical inertness [4]. Other criteria for the selection of important materials include thermodynamic resistance of the coating to thermally grown aluminum oxide at high temperatures, specific thermal conductivity, erosion resistance, and tendency to losses resulting from evaporation in the presence of water contained in the environment.

Our understanding of the TBC behavior control mechanisms has improved significantly after research and developments over the last two decades, but no unique upper coating has been found that would surpass YSZ; the balance of properties remain an issue. NASA still uses the developed basic upper layer. It was essentially a mother-nature gift after short-term development efforts, mainly those of NASA, based on the known properties of consolidated oxides used in the industry.

Defect cluster materials attract the most attention because of their low thermal conductivity and quite high thermal expansion coefficients. These materials do not cause serious problems during spraying and appear to be the most promising today [193].

The fastest progress is likely only in combination of intuition about crystalline structures and complementary simulations at the atomic level for experiments [2].

The multilayer structure concept is effective for improving the TBC thermal shock resistance because none of the materials satisfies all requirements. Compositions of low thermal conductivity, CeO_2–Y_2O_3, $Gd_2Zr_2O_7$, $Dy_2Zr_2O_7$, $Sm_2Zr_2O_7$, $La_2Ce_2O_7$, and $Sr(Zr_{0.9}Yb_{0.1})O_{2.95}$, will require the application of the YSZ base layer because of the chemical incompatibility with thermally grown oxide. This will complicate the process and increase the cost. The erosion and impact resistance of compositions with low thermal conductivity is lower than that of the YSZ TBCs. Comparisons of laboratory test data with engine testing results are required, but the experience in such efforts is still limited [189].

The thermal conductivity of the coating materials is limited to phonon scattering mechanics, which is due to the intrinsic properties of materials such as architecture, structure, and atomic bonding [194].

Ions and atoms with different ionic radii can also dissipate phonons by local deformation of the bonds and, thus, introduce the elastic strain fields into the lattice. Materials with a large average atomic mass, low Young's module, and randomly distributed point defects of sufficiently high density contribute to the reduction of the phonon free path and, consequently, to the reduction of thermal conductivity. In addition, nanosized-grain materials have lower thermal conductivity due to much more intense scattering of phonons by grain boundaries [171].

Impact damage caused by falling particles can be reduced by using multilayer architectures with required microstructure, which allows smoothing the stress distribution across the layers and minimizing the stress concentration at interfaces [195, 196]. Functional gradient coatings consist of multiphase composites, which demonstrate the smooth spatial change of components. This is achieved by applying a bond coating to the metal substrate, followed by the deposition of metal ceramic layers and upper ceramic layer. Tests that include the impact of a single particle are required. Measurement of properties such as hardness and fracture toughness at elevated temperatures will contribute to further understanding in this area.

The TBCs obtained using nanostructured raw materials have low thermal conductivity resulting from the presence of molten and porous nanodomains in their microstructure [197].

The conventional techniques for depositing protective coatings have somewhat negative effect on the properties of the metal substrate. In this case, it is desirable to use an ultrathin protective coating. Graphene, consisting of a single layer of carbon atoms connected in a 2D hexagonal network, is promising for such applications [160].

The need for repairing damaged TBCs and creating multilayer TBCs to ensure the exact sizes and concentration of doping admixtures calls for the use of sol–gel routes. These flexible and cost-effective processes are capable of producing a coating with uneven porosity. The sol–gel routes have already been used for the manufacture of sensors for TBCs [198].

Understanding the behavior of materials at high temperatures should be detailed using precise methods for measuring the properties (such as fracture toughness and hardness) at these temperatures. There is a need to measure the exact temperature on the surface and at the boundaries of TBC components.

Sensor thermal barrier coatings facilitate the remote measurement of temperature and wear within the coatings by incorporating an optically active material into the TBC [199–201]. Along with nondestructive examination methods, data will be obtained on the residual life of TBCs and the quality of their production process will be controlled [3]. Studies focusing on the interaction of YSZ and $Gd_2Zr_2O_7$ coatings with a molten $Na_2SO_4 + V_2O_5$ mixture have demonstrated that the coatings containing $Gd_2Zr_2O_7$ show higher corrosion resistance at 1050°C than the YSZ coating [168].

The impact of calcium–magnesium–aluminosilicate dust, which limits the TBC surface temperature to 1200°C, can be the weakest point. The main approaches in this area include the use of sealants [178] and application of sacrificial layers onto the YSZ TBCs [178, 179]. Reduction in CMAS damage at higher temperatures requires the selection and modification of the spraying processes at affordable cost. The rare-earth zirconates have been showed to be promising in this respect [3].

The scientific understanding of the TBC behavior in operation has evolved significantly in the last decade through collaboration between industry, governmental laboratories, and universities. Unfortunately, such collaborative efforts have slowed down, at least in the United States. The collaboration needs to be continued because future TBC systems for higher-temperature applications are likely to be very complex, including multifunctional multilayers that require multidisciplinary efforts.

Future TBC studies will allow, in addition to improvement in the chemical composition and development of deposition processes, better understanding of the destruction mechanisms, prediction of the TBC service life, more efficient use of sensors, probably embedded ones, and application of nondestructive quality assurance methods in the TBC production process.

Improvement of laboratory tests of components, including thermomechanical and thermochemical–mechanical tests, simulating the operating conditions of engines, will allow the full benefit of TBC advantages [189].

REFERENCES

1. R. A. Miller, "Current status of thermal barrier coating: an overview," *Surf. Coat. Technol.*, **30**, 1–11 (1987).

2. D. R. Clarke and S. R. Phillpot, "Thermal barrier coating materials," *Mater. Today*, 22–29 (2005).

3. V. Kumar and B. Kandasubramanian, "Processing and design methodologies for advanced and novel thermal barrier coatings for engineering application," *Particuology*, **27**, 1–29 (2016).

4. X. Q. Cao, R. Vassen, and D. Stoever, "Ceramic materials for thermal barrier coatings," *J. Eur. Ceram. Soc.*, **24**, 1–10 (2004).

5. D. Zhu, Y. L. Chen, and R. A. Miller, "Defect clustering and nano-phase structure characterization of multi-component rare earth oxide doped zirconia-yttria thermal barrier coatings," *Ceram. Eng. Sci. Proc.*, **24**, 525–534 (2003).

6. C. G. Levi, "Emerging materials and processes for thermal barrier systems," *Curr. Opin. Solid State Mater. Sci.*, **8**, No. 1, 77–91 (2004).

7. J. R. Nicholls, K. J. Lawson, A. Johnstone, and D. S. Rickerby, "Methods to reduce the thermal conductivity of EB–PVD TBCs," *Surf. Coat. Technol.*, **151–152**, 383–391 (2002).

8. D. Zhu and R. A. Miller, "Thermal conductivity and sintering behavior of advanced thermal barrier coatings," *Ceram. Eng. Sci. Proc.*, **23**, 457–468 (2002).

9. R. Vassen, X. Cao, F. Tietz, et al., "Zirconates as new materials for thermal barrier coatings," *J. Am. Ceram. Soc.*, **83**, 2023–2028 (2000).

10. J. Wu, X. Wei, N. P. Padture, et al., "Low-thermal-conductivity rare-earth zirconates for potential thermal barrier coating applications," *J. Am. Ceram. Soc.*, **85**, 3031 (2002).

11. Q. L. Li, X. Zh. Cui, S. Q. Li, et al., "Synthesis and phase stability of scandia, gadolinia, and ytterbia co-doped zirconia for thermal barrier coating application," *J. Therm. Spray Technol.*, **24**, 136–143 (2015).

12. K. Matsumoto, Y. Itoh, and Y. Ishiwata, "Thermal conductivity and sintering behavior of hafnia-based thermal barrier coating using EB-PVD," in: *Proc. Int. Gas Turb. Congress* (Tokyo, 2003, Nov. 2–7), Tokyo (2003), pp. 1–6.

13. U. Schulz, B. Saruhan, K. Fritscher, and C. Leyens, "Review on advanced EB–PVD ceramic top coats for TBC applications," *Int. J. Appl. Ceram. Technol.*, **1**, No. 4, 302–315 (2004).

14. M. N. Rahaman, J. R. Gross, R. E. Dutton, and H. Wang, "Phase stability, sintering, and thermal conductivity of plasma-sprayed ZrO_2–Gd_2O_3 compositions for potential thermal barrier coating applications," *Acta Mater.*, **54**, 1615–1621 (2006).

15. M. Matsumoto, H. Takayama, D. Yokoe, et al., "Thermal cycle behavior of plasma sprayed La_2O_3, Y_2O_3 stabilized ZrO_2 coatings," *Scr. Mater.*, **54**, 2035–2039 (2006).

16. Z.-G. Liu, J.-H. Ouyang, B.-H. Wang, et al., "Thermal expansion and thermal conductivity of $Sm_xZr_{1-x}O_{2-x}/2$ $(0.1 \leq x \leq 0.5)$ ceramics," *Ceram. Int.*, **35**, 791–796 (2009).

17. G. Di Girolamo, C. Blasi, M. Schioppa, and L. Tapfer, "Structure and thermal properties of heat treated plasma sprayed ceria–yttria co-stabilized zirconia coatings," *Ceram. Int.*, **85**, 3031–3035 (2002).

18. X. Song, M. Xie, X. Hao, et al., "Structure and thermal conductivity of $Zr_{1-x}Gd_xO_{2-x/2}$ solid solutions," *J. Alloys Compd.*, **497**, L5–L8 (2010).

19. H. Liu, S. Li, Q. Li, et al., "Microstructure, phase stability and thermal conductivity of plasma sprayed Yb_2O_3, Y_2O_3 co-stabilized ZrO_2 coatings," *Solid State Sci.*, **13**, 513–519 (2011).

20. M. R. Loghman-Estarkia, R. S. Razavib, H. Edrisa, et al., "Life time of new SYSZ thermal barrier coatings produced by plasma spraying method under thermal shock test and high temperature treatment," *Ceram. Int.*, **40**, 1404–1414 (2014).

21. L. Qu and K.-L. Choy, "Thermophysical and thermochemical properties of new thermal barrier materials based on Dy_2O_3–Y_2O_3 co-doped zirconia," *Ceram. Int.*, **40**, 11593–11599 (2014).

22. R. Vaßen, F. Tietz, G. Kerkhoff, and D. Stöver, "New materials for advanced thermal barrier coatings," in: J. Lecomte-Beckers, F. Schuber, and P. J. Ennis (eds.), *Proc. 6th Liége Conf. Materials for Advanced Power Engineering* (Forschungszentrum Jülich, Jülich, Germany, 1998), Jülich (1998), pp. 1627–1635.

23. J. Thornton and A. Majumdar, "Ceria precipitation and phase stability in zirconia based thermal barrier coatings," in: A. Ohmori (ed.), *Proc. 14th International Thermal Spray Conference: Thermal Spray–Current Status and Future Trends*, ASM International, Materials Park, OH, USA (1995), pp. 1075–1080.

24. R. L. Jones, "Development of hot-corrosion-resistant zirconia thermal barrier coatings," *Mater. High Temp.*, **9**, 228–236 (1991).

25. R. L. Jones, "Some aspects of the hot corrosion of thermal barrier coatings," *J. Therm. Spray Technol.*, **6**, No. 1, 77–84 (1997).

26. W. Ma and H. Dong, "Ceramic thermal barrier coating materials," in: *Thermal Barrier Coatings* (2011), pp. 25–52.

27. P. Ramaswamy, S. Seetharamu, K. R. Varma, and K. J. Rao, "Thermal shock characteristics of plasma sprayed mullite coatings," *J. Therm. Spray Technol.*, **7**, No. 4, 497–504 (1999).

28. M. J. Maloney, *Thermal Barrier Coating Systems and Materials,* US Patent No. 6,117.560 (2000).

29. V. P. Red'ko, *Physicochemical Study of $M_4Zr(Hf)_3O_{12}$ Compounds in the $ZrO_2(HfO_2)$–Rare Earth Oxide Systems* [in Russian], Author's Abstract of PhD Thesis, Kyiv (1990), p. 20.

30. W. Ma, Sh. Gong, H. Xu, and X. Cao, "The thermal cycling behavior of lanthanum–cerium oxide thermal barrier coating prepared by EB–PVD," *Surf. Coat. Technol.*, **200**, 5113–5118 (2006).

31. Q. Xu, W. Pan, J. Wang, et al., "Rare-earth zirconate ceramics with fluorite structure for thermal barrier coatings," *J. Am. Ceram. Soc.*, **89**, No. 1, 340–342 (2006).

32. L. Ling, X. Qiang, W. Fuchi, and Z. Hongsong, "Thermophysical properties of complex rare-earth zirconate ceramic for thermal barrier coatings," *J. Am. Ceram. Soc.*, **91**, No. 7, 2398–2401 (2008).

33. Z.-G. Liu, J.-H. Ouyang, Y. Zhou, and X.-L. Xia, "Electrical conductivity and thermal expansion of neodymium–ytterbium zirconate ceramics," *J. Power Sources*, **195**, 3261–3265 (2010).

34. K. S. Lee, K. I. Jung, Y. S. Heo, et al., "Thermal and mechanical properties of sintered bodies and EB-PVD layers of Y_2O_3 added $Gd_2Zr_2O_7$ ceramics for thermal barrier coatings," *J. Alloys Compd.*, **507**, 448–455 (2010).

35. Zh. Xu, L. He, X. Chen, et al., "Thermal cycling behavior of $La_2Zr_2O_7$ coating with the addition of Y_2O_3 by EB-PVD," *J. Alloys Compd.*, **508**, 85–93 (2010).

36. Ch. Wan, W. Zhang, Y. Wang, et al., "Glass-like thermal conductivity in ytterbium-doped lanthanum zirconate pyrochlore," *Acta Mater.*, **58**, 6166–6172 (2010).

37. B. Liu, J. Y. Wang, F. Z. Li, and Y. C. Zhou, "Theoretical elastic stiffness, structural stability, and thermal conductivity of $La_2T_2O_7$ (T = Ge, Ti, Sn, Zr, Hf) pyrochlore," *Acta Mater.*, **58**, 4369–4377 (2010).

38. H. Chen, Y. Liu, Y. Gao, et al., "Design, preparation, and characterization of graded YSZ/$La_2Zr_2O_7$ thermal barrier coatings," *J. Am. Ceram. Soc.*, **93**, No. 6, 1732–1740 (2010).

39. H. Zhao, M. R. Begley, A. Heuer, et al., "Reaction, transformation and delamination of samarium zirconate thermal barrier coatings," *Surf. Coat. Technol.*, **205**, 4355–4365 (2011).

40. H. Zhang, S. Liao, X. Dang, et al., "Preparation and thermal conductivities of $Gd_2Ce_2O_7$ and $(Gd_{0.9}Ca_{0.1})_2Ce_2O_{6.9}$ ceramics for thermal barrier coatings," *J. Alloys Compd.*, **509**, 1226–1230 (2011).

41. Zh. Xu, Sh. He, L. He, et al., "Novel thermal barrier coatings based on $La_2(Zr_{0.7}Ce_{0.3})_2O_7$/8YSZ double-ceramic-layer systems deposited by electron beam physical vapor deposition," *J. Alloys Compd.*, **509**, 4273–4283 (2011).

42. Ch. Wan, Zh. Qu, A. Du, and W. Pan, "Order–disorder transition and unconventional thermal conductivities of the $(Sm_{1-x}Yb_x)_2Zr_2O_7$ series," *J. Am. Ceram. Soc.*, **94**, No. 2, 592–596 (2011).

43. L. Liu, F. Wang, Zh. Ma, et al., "Thermophysical properties of $(Mg_xLa_{0.5x}Sm_{0.5})_2(Zr_{0.7}Ce_{0.3})_2O_{7x}$ (x = 0, 0.1, 0.2, 0.3) ceramic for thermal barrier coatings," *J. Am. Ceram. Soc.*, **94**, No. 3, 675–678 (2011).

44. K.-H. Kwak, B.-Ch. Shim, S.-M. Lee, et al., "Formation and thermal properties of fluorite-pyrochlore composite structure in $La_2(Zr_xCe_{1-x})_2O_7$ oxide system," *Mater. Lett.*, **65**, 2937–2940 (2011).

45. J. Feng, B. Xiao, C. L. Wan, et al., "Electronic structure, mechanical properties and thermal conductivity of $Ln_2Zr_2O_7$ (Ln = La, Pr, Nd, Sm, Eu and Gd) pyrochlores," *Acta Mater.*, **59**, 1742–1760 (2011).

46. G. Moskal, L. Swadzba, M. Hetmanczyk, et al., "Characterization of microstructure and thermal properties of $Gd_2Zr_2O_7$-type thermal barrier coating," *J. Eur. Ceram. Soc.*, **32**, 2025–2034 (2012).

47. G. Moskal, L. Swadzba, M. Hetmanczyk, et al., "Characterization of the microstructure and thermal properties of $Nd_2Zr_2O_7$ and $Nd_2Zr_2O_7$/YSZ thermal barrier coatings," *J. Eur. Ceram. Soc.*, **32**, 2035–2042 (2012).

48. Zh. Xu, L. He, R. Mu, et al., "Thermal cycling behavior of YSZ and $La_2(Zr_{0.7}Ce_{0.3})_2O_7$ as double-ceramic-layer systems EB-PVD TBCs," *J. Alloys Compd.*, **525**, 87–96 (2012).

49. H.-S. Zhang, X.-G. Chen, G. Li, et al., "Influence of Gd_2O_3 addition on thermophysical properties of $La_2Ce_2O_7$ ceramics for thermal barrier coatings," *J. Eur. Ceram. Soc.*, **32**, 3693–3700 (2012).

50. M. Zhao, X. Ren, and W. Pan, "Mechanical and thermal properties of simultaneously substituted pyrochlore compounds $(Ca_2Nb_2O_7)_x(Gd_2Zr_2O_7)_{1-x}$," *J. Eur. Ceram. Soc.*, **35**, 1055–1061 (2015).

51. A. Joulia, M. Vardelle, and S. Rossignol, "Synthesis and thermal stability of $Re_2Zr_2O_7$ (Re = La, Gd) and $La_2(Zr_{1-x}Ce_x)_2O_{7-\delta}$ compounds under reducing and oxidant atmospheres for thermal barrier coatings," *J. Eur. Ceram. Soc.*, **33**, 2633–2644 (2013).

52. H. Zhang, L. Guo, Y. Ma, et al., "Thermal cycling behavior of $(Gd_{0.9}Yb_{0.1})_2Zr_2O_7$/8YSZ gradient thermal barrier coatings deposited on Hf-doped NiAl bond coat by EB-PVD," *Surf. Coat. Technol.*, **258**, 950–955 (2014).

53. Y. Zhang, M. Xiea, F. Zhou, et al., "Low thermal conductivity in $La_2Zr_2O_7$ pyrochlore with a-site partially substituted with equimolar Yb_2O_3 and Er_2O_3," *Ceram. Int.*, **40**, 9151−9157 (2014).

54. L. Guo, H. Guo, H. Peng, and Sh. Gong, "Thermophysical properties of Yb_2O_3 doped $Gd_2Zr_2O_7$ and thermal cycling durability of $(Gd_{0.9}Yb_{0.1})_2Zr_2O_7$/YSZ thermal barrier coatings," *J. Eur. Ceram. Soc.*, **34**, 1255–1263 (2014).

55. Z.-G. Liu, W.-H. Zhang, J.-H. Ouyang, and Y. Zhou, "Novel double-ceramic-layer $(La_{0.8}Eu_{0.2})_2Zr_2O_7$/YSZ thermal barrier coatings deposited by plasma spraying. Part 2," *Ceram. Int.*, **40**, No. 7, 11277–11282 (2014).

56. M. Zhao, X. Ren, and W. Pan, "Mechanical and thermal properties of simultaneously substituted pyrochlore compounds $(Ca_2Nb_2O_7)_x(Gd_2Zr_2O_7)_{1-x}$," *J. Eur. Ceram Soc.*, **35**, 1055–1061 (2015).

57. X. Zhou, Z. Xu, X. Fan, et al., "$Y_4Al_2O_9$ ceramics as a novel thermal barrier coating material for high-temperature applications," *Mater. Lett.*, **134**, 146–148 (2014).

58. Y. Zhou, H. Xiang, and Z. Feng, "Theoretical investigation on mechanical and thermal properties of a promising thermal barrier material $Yb_3Al_5O_{12}$," *J. Mater. Sci. Technol.*, **30**, No. 7, 631–638 (2014).

59. K. Matsumoto, Y. Itoh, and T. Kameda, "EB-PVD process and thermal properties of hafnia-based thermal barrier coating," *Sci. Technol. Adv. Mater.*, **4**, 153–158 (2003).

60. M. Zhao, X. Ren, J. Yang, and W. Pan, "Thermomechanical properties of ThO_2-doped Y_2O_3 stabilized ZrO_2 for thermal barrier coatings," *Ceram. Int.*, **42**, 501–508 (2016).

61. R. Gadow and M. Lischka, "Lanthanum hexaaluminate—novel thermal barrier coatings for gas turbine applications," *Surf. Coat. Technol.*, **151–152**, 392–399 (2002).

62. W. Ma, D. E. Mack, R. Vaβen, and D. Stover, "Perovskite-type strontium zirconate as a new material for thermal barrier coatings," *J. Am. Ceram. Soc.*, **91**, No. 8, 2630–2635 (2008).

63. H. Liu, W. Zhao, Q. An, et al., "Nanomechanical properties and microstructure of ZrO_2/Al_2O_3 plasma sprayed coatings," *Mat. Sci. Eng. A*, **518**, 185–189 (2009).

64. A. Du, Ch. Wan, Zh. Qu, and W. Pan, "Thermal conductivity of monazite-type $REPO_4$ (RE = La, Ce, Nd, Sm, Eu, Gd)," *J. Am. Ceram. Soc.*, **92**, No. 11, 2687–2692 (2009).

65. X. Chen, Y. Zhang, X. Zhong, et al., "Thermal cycling behaviors of the plasma sprayed thermal barrier coatings of hexaluminates with magnetoplumbite structure," *J. Eur. Ceram. Soc.*, **30**, 1649–1657 (2010).

66. Z. Negahdari, M. Willert-Porada, and F. Scherm, "Thermal properties of homogenous lanthanum hexaaluminate/alumina composite ceramics," *J. Eur. Ceram. Soc.*, **30**, 3103–3109 (2010).

67. Y.-H. Wang, J.-H. Ouyang, and Z.-G. Liu, "Influence of dysprosium oxide doping on thermophysical properties of $LaMgA_{11}O_{19}$ ceramics," *Mater. Des.*, **31**, 3353–3357 (2010).

68. Ch. Wan, T. D. Sparks, P. Wei, and D. R. Clarke, "Thermal conductivity of the rare-earth strontium aluminates," *J. Am. Ceram. Soc.*, **93**, No. 5, 1457–1460 (2010).

69. F. Yang, X. Zhao, and P. Xiao, "Thermal conductivities of YSZ/Al_2O_3 composites," *J. Eur. Ceram. Soc.*, **30**, 3111–3116 (2010).

70. Q. Yu, Ch. Zhou, H. Zhang, and F. Zhao, "Thermal stability of nanostructured 13 wt.% Al_2O_3–8 wt.% Y_2O_3–ZrO_2 thermal barrier coatings," *J. Eur. Ceram. Soc.*, **30**, 889–897 (2010).

71. E. Garcia, J. Mesquita-Guimaraes, M. I. Osendi, and P. Miranzo, "Thermal conductivity in mullite/ZrO_2 composite coatings," *Ceram. Int.*, **36**, 1609–1614 (2010).

72. X. Xie, H. Guo, S. Gong, and H. Xu, "Thermal cycling behavior and failure mechanism of $LaTi_2Al_9O_{19}$/YSZ thermal barrier coatings exposed to gas flame," *Surf. Coat. Technol.*, **205**, 4291–4298 (2011).

73. X. Chen, Y. Zhao, W. Huang, et al., "Thermal aging behavior of plasma sprayed $LaMgAl_{11}O_{19}$ thermal barrier coating," *J. Eur. Ceram. Soc.*, **31**, 2285–2294 (2011).

74. J. Frodelius, E. M. Johansson, J. M. Cordoba, et al., "Annealing of thermally sprayed Ti_2AlC coatings," *Int. J. Appl. Ceram. Technol.*, **8**, No. 1, 74–84 (2011).

75. J. Hostasa, W. Pabst, and J. Matejicek, "Thermal conductivity of Al_2O_3–ZrO_2 composite ceramics," *J. Am. Ceram. Soc.*, **94**, No. 12, 4404–4409 (2011).

76. Y.-H. Wang, Z.-G. Liu, J.-H. Ouyang, et al., "Preparation and thermophysical properties of $LaMgAl_{11}O_{19}$–$Yb_3Al_5O_{12}$ ceramic composites," *Ceram. Int.*, **37**, 2489–2493 (2011).

77. L.-D. Zhao, Y.-L. Pei, Y. Liu, et al., "$InFeZnO_4$ as promising thermal barrier coatings," *J. Am. Ceram. Soc.*, **94**, No. 6, 1664–1666 (2011).

78. M. Noor-A-Alam and C. V. Ramana, "Structure and thermal conductivity of yttria-stabilized hafnia ceramic coatings grown on nickel-based alloy," *Ceram. Int.*, **38**, 2957–2961 (2012).

79. H. Dong, D. Wang, Y. Pei, et al., "Optimization and thermal cycling behavior of $La_2Ce_2O_7$ thermal barrier coatings," *Ceram. Int.*, **39**, 1864−1870 (2013).

80. L. He, X. Zhou, B. Zhong, et al., "Phase evolution, interdiffusion, and failure of $La_2(Zr_{0.7}Ce_{0.3})_2O_7$/YSZ thermal barrier coatings prepared by electron beam-physical vapor deposition," *J. Alloys Compd.*, **624**, 137–147 (2015).

81. J. S. V. Sluytman, S. Krämer, V. K. Tolpygo, and C. G. Levi, "Microstructure evolution of ZrO_2–$YbTaO_4$ thermal barrier coatings," *Acta Mater.*, **96**, 133−142 (2015).

82. X. Wang, H. Xiang, X. Sun, et al., "Mechanical properties and damage tolerance of bulk $Yb_3Al_5O_{12}$ ceramic," *J. Mater. Sci. Technol.*, **31**, 369−374 (2015).

83. M. Zhao, X. Ren, J. Yang, and W. Pan, "Thermomechanical properties of ThO_2-doped Y_2O_3 stabilized ZrO_2 for thermal barrier coatings," *Ceram. Int.*, **42**, 501−508 (2016).

84. C. Xiao, H. Zhang, H. S. Zhang, et al., "$Ce_{1-x}Sm_xO_{2-x/2}$—a novel type of ceramic materials for thermal barrier coatings," *J. Adv. Ceram.*, **5**, No. 3, 244–252 (2016).

85. S. M. Lakiza and L. M. Lopato, "Stable and metastable phase relations in the system alumina–zirconia–yttria," *J. Am. Ceram. Soc.*, **80**, No. 4, 893–902 (1997).

86. S. Lakiza, O. Fabrichnaya, M. Zinkevich, and F. Aldinger, "On the phase relations in the ZrO_2–$YO_{1.5}$–$AlO_{1.5}$ system," *J. Alloys Compd.*, **420**, 237–245 (2006).

87. S. M. Lakiza and L. M. Lopato, "Phase diagram of the Al_2O_3–ZrO_2–La_2O_3 system," *J. Eur. Ceram. Soc.*, **25**, No. 8, 1373–1380 (2005).

88. S. Lakiza and L. Lopato, "Phase diagram of the alumina–zirconia–samaria system," *J. Am. Ceram. Soc.*, **89**, No. 11, 3516–3521 (2006).

89. S. M. Lakiza and L. M. Lopato, "Phase diagram of the Al_2O_3–ZrO_2–Nd_2O_3 system," *J. Eur. Ceramic Soc.*, **26**, 3725–3732 (2006).

90. S. Lakiza, O. Fabrichnaya, Ch. Wang, et al., "Phase diagram of the ZrO_2–Gd_2O_3–Al_2O_3 system," *J. Eur. Ceram. Soc.*, **26**, 233–246 (2006).

91. S. M. Lakiza and L. M. Lopato, "Phase diagram of the Al_2O_3–ZrO_2–Er_2O_3 system," *J. Eur. Ceramic Soc.*, **28**, No. 12, 2389–2397 (2008).

92. S. M. Lakiza, V. P. Red'ko, and L. M. Lopato, "The Al_2O_3–ZrO_2–Yb_2O_3 phase diagram. I. Isothermal sections at 1250 and 1650°C," *Powder Metall. Met. Ceram.*, **47**, Nos. 3–4, 202–210 (2008).

93. S. M. Lakiza and L. M. Lopato, "Phase diagrams of the systems Al_2O_3–ZrO_2–$Ln(Y)_2O_3$ as a source of multiphase eutectics for creating composite structural and functional materials," *J. Eur. Ceram. Soc.*, **31**, 1293–1303 (2011).

94. S. M. Lakiza, Ya. S. Tishchenko, V. P. Red'ko, and L. M. Lopato, "The Al_2O_3–HfO_2–La_2O_3 phase diagram. II. Phase equilibria at 1250 and 1600°C," *Powder Metall. Met. Ceram.*, **50**, Nos. 5–6, 345−349 (2011).

95. J. S. Tyschenko, S. M. Lakiza, and E. V. Dudnik, "Phase diagrams of the Al_2O_3−TiO_2−Ln_2O_3 (Ln = La, Gd, Er, and Y) systems as the basis for creating new structural and functional eutectic ceramics," in: *Abstracts DSECV (April 3–7, 2016, Warsaw, Poland)*, Warsaw (2016), p. 68.

96. Ya. S. Tyshchenko, S. M. Lakiza, V. P. Red'ko, and O. V. Dudnik, "Isothermal sections of the Al_2O_3–TiO_2–Y_2O_3 phase diagram at 1550 and 1400°C," *Powder Metall. Met. Ceram.*, **55**, No. 11–12, 698−706 (2017).

97. J. R. Nicholls, M. J. Deakin, and D. S. Rickerby, "A comparison between the erosion behavior of thermal spray and electron-beam physical vapor deposition thermal barrier coatings," *Wear*, **233–235**, 352–361 (1999).

98. U. Schulz, C. Leyens, K. Fritscher, et al., "Some recent trends in research and technology of advanced thermal barrier coatings," *Aerospace Sci. Technol.*, **7**, 73–80 (2003).

99. S. M. Meier and D. K. Gupta, "The evolution of thermal barrier coatings in gas turbine engine applications," *Trans. ASME*, **116**, 250–257 (1994).

100. B. P. Bewlay, M. R. Jackson, J.-C. Zhao, et al., "Ultrahigh temperature Nb-silicide based composites," *MRS Bull.*, **28**, 646–653 (2003).

101. D. V. Rigney, A. F. Maricocchi, D. J. Wortman, et al., *Method for Forming a Thermal Barrier Coating System*, US Patent No. 6,447,854 (2002).

102. J. D. Rigney and D. J. Wortman, *Physical Properties of Thermal Barrier Coatings Using Electron Beam-Physical Vapor Deposition*, US Patent No. 6,620,465 (2003).

103. J. R. Nicholls, K. J. Lawson, D. S. Rickerby, and P. Morell, "Advanced processing of TBCs for reduced thermal conductivity," in: *Proc. 85th Meeting of the Advisory Group for Aerospace Research and Development*, AGARD, Structures and Materials Panel, Aalborg, Denmark (1998), pp. 6.1–6.9.

104. Y. P. Jaslier, A. H. L. Malle, J.-P. Huchin, et al., *Ceramic Heat Barrier Coating Having Low Thermal Conductivity and Process for the Deposition of Said Coating*, US Patent No. 6,251,504,B1 (2001).

105. G. H. Marijnissen, A. H. F. Van Lieshout, G. J. Ticheler, et al., *Thermal Barrier Coating System Ceramic Structure*, US Patent No. 5,876,860 (1999).

106. T. E. Strangman, "Thermal barrier coatings for turbine airfoils," *Thin Solid Films*, **127**, 93–105 (1985).

107. D. D. Hass, P. A. Parrish, and H. N. G. Wadley, "Electron beam directed vapor deposition of thermal barrier coatings," *J. Vac. Sci. Technol. A*, **16**, No. 6, 3396–3401 (1998).

108. T. A. Taylor, *Thermal Barrier Coating for Substrates and Process for Producing It*, US Patent No. 5,073,433 (1991).

109. K. Kokini, A. Banerjee, and T. A. Taylor, "Thermal fracture of interfaces in precracked thermal barrier coatings," *Mater. Sci. Eng.*, **A323**, 70 (2002).

110. S. D. Graham, M. F. De Sol, M. L. Smith, et al., *Dense Vertically Cracked Thermal Barrier Coating Process to Facilitate Postcoat Surface Finishing*, US Patent No. 6,432,487 (2000).

111. T. Bhatia, A. Ozturk, L. Xie, et al., "Mechanisms of ceramic coating deposition in solution precursor plasma spray," *J. Mater. Res.*, **17**, 2363–2372 (2002).

112. M. Gell, L. Xie, X. Ma, et al., "Highly durable thermal barrier coatings made by the solution precursor plasma spray process," *Surf. Coat. Technol.*, **177–178**, 97–102 (2004).

113. N. P. Padture, K. W. Schlichting, T. Bhatia, et al., "Toward durable thermal barrier coatings with novel microstructures deposited by solution precursor plasma spray," *Acta Mater.*, **49**, 2251–2257 (2001).

114. H. N. G. Wadley, X. W. Zhou, R. N. Johnson, and M. Neurock, "Mechanisms, models, and methods of vapor deposition," *Progr. Mater. Res.*, **46**, 329–377 (2001).

115. J. Cho, S. G. Terry, R. LeSar, and C. G. Levi, "A kinetic Monte Carlo simulation of film growth by physical vapor deposition on rotating substrates," *Mater. Sci. Eng. A*, No. 1−2, 390−401 (2005).

116. O. Vasilyev, M. Brychevskyi, I. Brodnikovskyi, et al., "EB-PVD helium-tight zirconia ceramic coating on porous ceramic substrate," *Zastita Mater.*, **57**, No. 2, 244−252 (2016).

117. S. G. Terry, *Evolution of Microstructure during the Growth of Thermal Barrier Coatings by Electron-Beam Physical Vapor Deposition: Doctoral Dissertation in Materials*, University of California, Santa Barbara, CA, USA (2001).

118. U. Schulz, S. G. Terry, and C. G. Levi, "Microstructure and texture of EBPVD TBCs grown under different rotation modes," *Mater. Sci. Eng.*, **A360**, 319–329 (2003).

119. A. Kulkarni, Z. Wang, T. Nakamura, et al., "Comprehensive microstructural characterization and predictive property modeling of plasma sprayed zirconia coatings," *Acta Mater.*, **51**, 2457–2475 (2003).

120. V. G. Varanasi, T. M. Besmann, R. L. Hyde, et al., "MOCVD of YSZ coatings using β-diketonate precursors," *Mater. Sci. Eng. A*, **528**, No. 3, 978–985 (2011).

121. A. Majumdar and S. Jana, "Yttria doped zirconia in glassy matrix useful for thermal barrier coating," *Mater. Lett.*, **44**, No. 3, 197–202 (2000).

122. J. Fenech, C. Viazzi, J. P. Bonino, et al., "Morphology and structure of YSZ powders: comparison between xerogel and aerogel," *Ceram. Int.*, **35**, No. 8, 3427–3433 (2009).

123. L. Pin, C. Pilgrim, J. Feist, et al., "Characterization of thermal barrier sensor coatings synthesized by sol–gel route," *Sens. Actuators A: Phys.*, **199**, 289–296 (2013).

124. A. Hospach, G. Mauer, R. Vaßen, and D. Stöver, "Columnar-structured thermal barrier coatings (TBCs) by thin film low-pressure plasma spraying (LPPS-TF)," *J. Therm. Spray Technol.*, **20**, Nos. 1–2, 116–120 (2011).

125. D. R. Clarke and C. G. Levi, "Materials design for the next generation of thermal barrier coatings," *Ann. Rev. Mater. Res.*, **33**, 383–417 (2003).

126. Y. Wang, M. X. Li, and H. L. Suo, "Mechanical properties of YSZ thermal barrier coatings with segmented structure," *Surf. Eng.*, **28**, No. 5, 329−332 (2012).

127. R. Vaßen, Y. Kagawa, R. Subramanian, et al., "Testing and evaluation of thermal-barrier coatings," *MRS Bull.*, **37**, No. 10, 891−898 (2012).

128. U. Schulz, K. Fritscher, C. Leyens, and M. Peters, "High-temperature aging of EB-PVD TBCs," *Ceram. Eng. Sci. Proc.*, **22**, No. 4, 347–356 (2001).

129. K. Fritscher, F. Szücs, U. Schulz, et al., "Impact of thermal exposure of EBPVD TBCs on Young`s modulus and sintering," *Ceram. Eng. Sci. Proc.*, **23–24**, 341–352 (2002).

130. C. A. Johnson, J. A. Ruud, R. Bruce, and D. Wortman, "Relationships between residual stress, microstructure and mechanical properties of electron beam physical vapor deposition TBCs," *Surf. Coat. Technol.*, **108–109**, 80–85 (1998).

131. U. Schulz, K. Fritscher, C. Leyens, and M. Peters, "Influence of processing on microstructure and performance of electron beam physical vapor deposition (EB-PVD) TBCs," *J. Eng. Gas Turbines Power*, **124**, No. 2, 229–234 (2002).

132. T. A. Dobbins, A. J. Allen, J. Ilavsky, et al., "Recent developments in the characterization of anisotropic void populations in TBCs using ultra-small angle x-ray scattering," *Ceram. Eng. Sci. Proc.*, **24**, No. 3, 517–521 (2003).

133. A. A. Kulkarni, H. Herman, J. Almer, et al., "Depth-resolved porosity investigation of EB−PVD TBCs using high-energy X-rays," *J. Am. Ceram. Soc.*, **87**, No. 2, 268–274 (2004).

134. D. Zhu, R. A. Miller, B. A. Nagaraj, and R. W. Bruce, "Thermal conductivity of EB−PVD TBCs evaluated by a steady-state laser heat flux technique," *Surf. Coat. Technol.*, **138**, No. 1, 1−8 (2001).

135. R. B. Dinwiddie, S. C. Beecher, and W. D. Porter, "The effect of thermal aging on the thermal conductivity of plasma sprayed and EB-PVD TBCs," *Amer. Soc. Mech. Eng. (ASME)* (1996).

136. A. Azzopardi, R. Mevrel, B. Saint-Ramond, et al., "Influence of aging on structure and thermal conductivity of Y-PSZ and Y-FSZ EBPVD coatings," *Surf. Coat. Technol.*, **177–178**, 131–139 (2004).

137. V. Lughi, V. K. Tolpygo, and D. R. Clarke, "Microstructural aspects of the sintering of TBCs," *Mater. Sci. Eng.*, **368**, No. 1–2, 212–221 (2004).

138. U. Schulz, "Phase transformation in EB-PVD yttria partially stabilized zirconia TBCs during annealing," *J. Amer. Ceram. Soc.*, **83**, No. 4, 904–910 (2000).

139. Y. H. Sohn, R. R. Biederman, R. D Sisson, et al., "Isothermal oxidation of physical vapor deposited partially stabilized zirconia TBCs," *J. Mater. Eng. Perform.*, **3**, No. 1, 55–60 (1994).

140. R. W. Bruce, D. J. Wortman, R. Viguie, and D. Skelly, *TBC System*, US Patent No. 5,981,088 (1999).

141. U. Schulz, J. Münzer, and U. Kaden, "Influence of deposition conditions on density and microstructure of EB-PVD TBCs," *Ceram. Eng. Sci. Proc.*, **23–24**, 353–360 (2002).

142. K. Fritscher and W. Bunk, "Density graded TBCs processed by EB-PVD," in: M. Yamanouchi et al. (ed.), *First Int. Symp. Functionally Gradient Materials, FGM90, Functionally Gradient Materials Forum*, Sendai, Japan (1990), pp. 91–96.

143. D. L. Youchison, M. A. Gallis, R. E. Nygren, et al., "Effects of ion beam assisted deposition, beam sharing and pivoting in EB−PVD processing of graded TBCs," *Surf. Coat. Technol.*, **177–178**, 158–164 (2004).

144. W. Beele, G. Marijnissen, E. Vergeldt, et al., "Evaluation of low thermal conductivity ceramic TBCs for aero-engine turbine blades by the herring bone process," in: *Forum Technol. Advanced Coatings for High Temperatures*, Nice (2002), pp. 1–7.

145. K. J. Lawson, J. R. Nicholls, and D. S. Rickerby, "Thermal conductivity and ceramic microstructure," in: D. R. J. Nicholls and D. Allen (eds.), *High Temperature Surface Engineering*, The Institute of Materials, London, UK (1997).

146. M. Kolloos and G. Marijnissen, *Burner Rig Testing of Herringbone EB−PVD TBCs*, NLR, German Aerospace Center, Turbomat, Bonn, Germany (2002), pp. 18–21.

147. D. D. Hass, A. J. Slifka, and H. N. G. Wadley, "Low thermal conductivity vapor deposited zirconia microstructures," *Acta Mater.*, **49**, No. 6, 973–983 (2001).

148. S. Gu, T. J. Lu, D. D. Hass, and H. N. G. Wadley, "Thermal conductivity of zirconia coatings with zig-zag pore microstructures," *Acta Mater.*, No. 13, 2539–2547 (2001).

149. U. Schulz, K. Fritscher, H. J. Rätzer-Scheibe, et al., "Thermocyclic behavior of microstructurally modified EB−PVD TBCs," *Mater. Sci. Forum*, 957–964 (1997).

150. J. R. Nicholls, K. J. Lawson, A. Johnstone, and D. Rickerby, "Low thermal conductivity EB-PVD TBCs," *Mater. Sci. Forum*, **369–372**, 595–606 (2001).

151. Jo. Singh, D. E. Wolfe, and Ja. Singh, "Architecture of TBCs produced by electron beam-physical vapor deposition (EB-PVD)," *J. Mater. Sci.*, **37**, No. 15, 3261–3267 (2002).

152. J. Singh, D. E. Wolfe, R. A. Miller, et al., "Tailored microstructure of zirconia and hafnia-based TBCs with low thermal conductivity and high hemispherical reflectance by EB-PVD," *J. Mater. Sci.*, **39**, No. 6, 1975–1985 (2004).

153. R. Subramanian and S. M. Sabol, *TBC Resistant to Sintering*, US Patent No. 6,203,927,B1 (2001).

154. T. E. Strangmann, *Durable TBC*, US Patent No. 6395343/5562998 (2002).

155. R. A. Miller, W. J. Brindley, J. G. Goedjen, et al., "The effect of silica on the cyclic life of a zirconia–yttria thermal barrier coating," in: C. C. Berndt and S. Sampath (eds.), *Proc. 7th Nat. Thermal Spray Conf. Thermal Spray in Industrial Applications* (Massachusetts, USA, June 1994), ASM International, Materials Park, Ohio, USA (1994), pp. 49–54.

156. Y. He, K. N. Lee, S. Tewari, and R. A. Miller, "Development of refractory silicate-yttria stabilized zirconia dual-layer thermal barrier coatings," *J. Therm. Spray Technol.*, **9**, No. 1, 59–67 (2000).

157. M. P. Borom, C. A. Johnson, and L. A. Peluso, "Role of environment deposits and operating surface temperature in spallation of air plasma sprayed thermal barrier coatings," *Surf. Coat. Technol.*, **86–87**, No. 1, 116–126 (1996).

158. I. Gurrappa, "Thermal barrier coatings for hot corrosion resistance of CM 247 LC superalloy," *J. Mater. Sci. Lett.*, **17**, No. 5, 1267–1269 (1998).

159. S. Y. Park, J. H. Kim, M. C. Kim, et al., "Microscopic observation of degradation behavior in yttria and ceria stabilized zirconia thermal barrier coatings under hot corrosion," *Surf. Coat. Technol.*, **190**, No. 2–3, 357–366 (2005).

160. V. Kumar and K. Balasubramanian, "Progress update on failure mechanisms of advanced thermal barrier coatings: a review," *Progr. Org. Coat.*, **90**, 54–82 (2016).

161. R. L. Jones, "Hot corrosion resistance of scandia stabilized zirconia coatings," *Ceram. Trans.*, **10**, 291–308 (1990).

162. R. L. Jones and D. Mess, "India as a hot corrosion-resistant stabilizer for zirconia," *J. Am. Ceram. Soc.*, **75**, No. 7b, 1818–1821 (1992).

163. Zh. Chen, N. Q. Wu, J. Singh, and S. X. Mao, "Effect of Al_2O_3 overlay on hot-corrosion behavior of yttria-stabilized zirconia coating in molten sulfate-vanadate salt," *Thin Solid Films*, **22**, No. 1–2, 46–52 (2003).

164. C. Batista, A. Portinha, R. M. Ribeiro, et al., "Evaluation of laser-glazed plasma-sprayed thermal barrier coatings under high temperature exposure to molten salts," *Surf. Coat. Technol.*, **200**, 6783–6791 (2006).

165. B. R. Marple, J. Voyer, M. Thibodeau, et al., "Hot corrosion of lanthanum zirconate and partially stabilized zirconia thermal barrier coatings," *J. Eng. Gas Turbines Power*, **128**, 144–152 (2006).

166. Z. Xu, L. He, R. Mu, et al., "Hot corrosion behavior of $La_2Zr_2O_7$ with the addition of Y_2O_3 thermal barrier coatings in contacts with vanadate–sulfate salts," *J. Alloys Compd.*, **504**, No. 2, 382–385 (2010).

167. Zh.-G. Liu, J.-H. Ouyang, Y. Zhou, and S. Li, "High-temperature hot corrosion behavior of gadolinium zirconate by vanadium pentoxide and sodium sulfate in air," *J. Eur. Ceram. Soc.*, **30**, 2707–2713 (2010).

168. M. H. Habibi, L. Wang, and S. M. Guo, "Evolution of hot corrosion resistance of YSZ, $Gd_2Zr_2O_7$, and $Gd_2Zr_2O_7$+YSZ composite thermal barrier coatings in Na_2SO_4+V_2O_5 at 1050°C," *J. Eur. Ceram. Soc.*, **32**, 1635–1642 (2012).

169. P. Mohan, B. Yuan, T. Patterson, et al., "Degradation of yttria-stabilized zirconia thermal barrier coatings by vanadium pentoxide, phosphorous pentoxide, and sodium sulfate," *J. Am. Ceram. Soc.*, **90**, 3601–3607 (2007).

170. X. H. Zhong, Y. M. Wang, Z. H. Xu, et al., "Hot-corrosion behaviors of overlay-clad yttria-stabilized zirconia coatings in contact with vanadate–sulfate salts," *J. Eur. Ceram. Soc.*, **30**, 1401–1408 (2010).

171. D. R. Clarke, M. Oechsner, and N. P. Padture, "Thermal-barrier coatings for more efficient gas-turbine engines," *MRS Bull.*, **37**, 891–898 (2012).

172. S. Kramer, J. Yang, C. G. Levi, and C. A. Johnson, "Thermochemical interaction of thermal barrier coatings with molten CaO–MgO–Al$_2$O$_3$–SiO$_2$ (CMAS) deposits," *J. Am. Ceram. Soc.*, **89**, No. 10, 3167–3175 (2006).

173. A. Aygun, A. L. Vasiliev, N. P. Padture, and X. Ma, "Novel thermal barrier coatings that are resistant to high-temperature attack by glassy deposits," *Acta Mater.*, **55**, No. 20, 6734–6748 (2007).

174. A. G. Evans and J. W. Hutchinson, "The mechanics of coating delamination in thermal gradients," *Surf. Coat. Technol.*, **201**, No. 18, 7905–7916 (2007).

175. J. M. Drexler, A. D. Gledhill, K. Shinoda, et al., "Jet engine coatings for resisting volcanic ash damage," *Adv. Mater.*, **23**, 2419–2424 (2011).

176. A. D. Gledhill, K. M. Reddy, J. M. Drexler, et al., "Mitigation of damage from molten fly ash to air-plasma-sprayed thermal barrier coatings," *Mater. Sci. Eng. A*, **258**, No. 24, 7214–7221 (2011).

177. J. M. Drexler, A. L. Ortiz, and N. P. Padture, "Composition effects of thermal barrier coating ceramics on their interaction with molten Ca–Mg–Al–Silicate (CMAS) glass," *Acta Mater.*, **60**, 5437–5447 (2012).

178. R. Darolia and B. A. Nagaraj, *Novel Thermal Barrier Coatings That Are Resistant to High-Temperature Attack by Glassy Deposits*, US Patent No. 6,720,038 (2004).

179. W. C. Hasz, C. A. Johnson, and M. P. Borom, *Coatings by Fuel Impurities and CMAS: Thermochemical Interactions and Mitigation*, US Patent No. 5,660,885 (1997).

180. D. L. Poerschke and C. G. Levi, "Effects of cation substitution and temperature on the interaction between thermal barrier oxides and molten CMAS," *J. Eur. Ceram. Soc.*, **35**, 681–691 (2015).

181. W. Braue and P. Mechnich, "Recession of an EB-PVD YSZ coated turbine blade by CaSO$_4$ and Fe, Ti-rich CMAS-type deposits," *J. Am. Ceram. Soc.*, **94**, No. 12, 4483–4489 (2011).

182. J. Ito and C. Frondel, "Synthetic zirconium and titanium garnets," *Am. Mineral.*, **52**, 773–781 (1967).

183. P. Mechnich, W. Braue, and U. Schulz, "High-temperature corrosion of EB-PVD yttria partially stabilized zirconia thermal barrier coatings with an artificial volcanic ash overlay," *J. Am. Ceram. Soc.*, **94**, No. 3, 925–931 (2011).

184. M. Peters, B. Saruhan-Brings, and U. Schulz, "Advanced coatings for blades of future aero engines," in: *Proc. Eur. Air Space Conf.* (October 26–29, 2009, CEAS, Manchester, UK), Manchester (2009), pp. 26–29.

185. S. Kramer, J. Yang, and C. G. Levi, "Infiltration–inhibiting reaction of gadolinium zirconate thermal barrier coatings with CMAS melts," *J. Am. Ceram. Soc.*, **91**, 576–583 (2008).

186. D. A. Litton, K. W. Schlichting, M. Freling, et al., *Mitigation of Damage from Molten Fly Ash to Air-Plasma*, US Patent No. 7,662,489 (2010).

187. M. Freling, K. W. Schlichting, M. J. Maloney, et al., *CMAS-Resistant Plasma Sprayed Thermal Barrier Coatings Based on Y$_2$O$_3$-Stabilized ZrO$_2$*, US Patent No. 7,785,722 (2010).

188. J. M. Drexler, A. D. Gledhill, K. Shinoda, et al., "Air-plasma-sprayed thermal barrier coatings that are resistant to high-temperature attack by glassy deposits," *Adv. Mater.*, **23**, 2419–2424 (2011).

189. R. Darolia, "Thermal barrier coatings technology: critical review, progress update, remaining challenges and prospects," *Int. Mater. Rev.*, **58**, No. 6, 315–348 (2013).

190. M. J. Stiger, N. M. Yanar, R. W. Jackson, et al., "Development of intermixed zones of alumina/zirconia in thermal barrier coating systems," *Metall. Mater. Trans. A*, **38**, No. 4, 848–857 (2007).

191. W. Beele, G. Marijnissen, and A. V. Lieshout, "The evolution of thermal barrier coatings—status and upcoming solutions for today's key issues," *Surf. Coat. Technol.*, **120–121**, 61–67 (1999).

192. Q. Xu, W. Pan, J. Wang, et al., "Preparation and thermophysical properties of Dy$_2$Zr$_2$O$_7$ ceramic for thermal barrier coatings," *Mater. Lett.*, **59**, No. 22, 2804–2807 (2005).

193. R. Vaßen, M. O. Jarligo, T. Steinke, et al., "Overview on advanced thermal barrier coatings," *Surf. Coat. Technol.*, **205**, 938–942 (2010).

194. P. G. Klemens and M. Gell, "Thermal conductivity of thermal barrier coatings," *Mater. Sci. Eng. A*, **245**, No. 2, 143–149 (1998).

195. A. Mimaroglu, E. Çelik, and E. Avci, "Fracture analysis for ZrO_2–GG ceramic coatings using finite element technique," in: *Proc. 5th Combustion Symp.* (July 1997, Bursa, Turkey), Bursa (1997), pp. 526–534.

196. H. D. Steffens, B. Wielage, and J. Drozak, "Interface phenomena and debonding mechanics of thermally sprayed metal and ceramic composites," *Surf. Coat. Technol.*, **45**, 291–308 (1991).

197. C. Amaya, J. C. Caicedo, J. M. Yáñez-Limón, et al., "Non-destructive method for determination of thermal conductivity of YSZ coatings deposited on Si substrates," *Mater. Chem. Phys.*, **136**, No. 22, 917–924 (2012).

198. L. Pin, Ch. Pilgrim, J. Feist, et al., "Characterization of thermal barrier sensor coatings synthesized by sol–gel route," *Sens. Actuators A: Phys.*, **199**, 289–296 (2013).

199. K. L. Choy, A. Heyes, and J. Feist, *Thermal Barrier Coating with Thermoluminescent Indicator Material Embedded Therein*, WO Patent No. WO/2000/006,796 (2000).

200. J. I. Eldridge, T. J. Bencic, S. W. Allison, and D. L. Beshears, "Depth-penetrating temperature measurements of thermal barrier coatings incorporating thermographic phosphors," *J. Therm. Spray Technol.*, **13**, No. 1, 44–50 (2004).

201. R. Steenbakker, J. Feist, R. Wellman, and J. Nicholls, "Sensor thermal barrier coatings: remote in situ condition monitoring of EB–PVD coatings at elevated temperatures," *J. Eng. Gas Turbines Power*, **131**, No. 4, 041301– 041309 (2009).